






# Novel Approximate Distribution of the Generalized Turbulence Channels for MIMO FSO Communications

Wafaa M. R. Shakir , *Member, IEEE*, Ali S. Mahdi, Hani Hamdan, Jinan Charafeddine , Haitham Al Satai , Radouane Akrache , Samir Haddad , and Jinane Sayah

**Abstract**—In this article, we develop an innovative series representation for the sum of Rician non-zero boresight pointing error random variates based on the  $\kappa - \mu$  distribution, which is suitable for multiple-input multiple-output (MIMO) transmission for the first time. Then, using this new representation, we introduce a novel closed-form probability density function (PDF) approximation for the sum of Gamma-Gamma random variates with generalized pointing errors and atmospheric attenuation of MIMO free-space optical (FSO) communications. Statistical Kolmogorov-Smirnov tests confirm the accuracy of this approximation over a wide range of channel conditions. The significance of this approximation is emphasized by deriving closed-form expressions for the ergodic capacity, outage probability, and average bit error rate (BER) using Meijer's G-function. This article provides a comprehensive analysis of the performance of MIMO FSO systems utilizing the equal gain combining (EGC) diversity technique under various conditions, such as different numbers of transmitter and receiver, turbulence intensities, the effects of non-zero boresight pointing errors, and path attenuation. The results show that using MIMO technology with more transmitters and receivers significantly improves the performance of FSO communication compared to other diversity techniques, including single input single output (SISO), and multiple input single output (MISO) systems. Detailed evaluations of the ergodic capacity, outage probability, and average BER performance at high signal-to-noise ratios provide additional insights.

Monte-Carlo simulation results demonstrate the accuracy of the proposed approach.

**Index Terms**—Multiple-input multiple-output (MIMO), free-space optical (FSO) communications, Gamma-Gamma turbulence, non-zero boresight pointing errors, Rician distribution, atmospheric attenuation, equal gain combining, Kolmogorov-Smirnov statistical tests.

## I. INTRODUCTION

**F**UTURE wireless technologies that go beyond the capabilities of 5th generation (5G) networks promise significant advances. These next-generation networks will offer exceptional data transfer rates, a wide range of broadband services, adaptable bandwidth options, and versatile communication solutions for a wide range of user needs. Wireless optical technologies critical to meeting future communication networks' data transmission requirements include free-space optical (FSO) technology. FSO offers several advantages, including cost efficiency, ease of deployment, high bandwidth capacity, and improved security [1]. However, despite these merits, the widespread adoption of FSO has been hampered by limitations in long-range applications. These limitations are due to atmospheric turbulence, which causes signal fading, attenuation due to factors such as fog, and pointing errors during signal transmission [2].

There are a variety of statistical models to describe scintillation effects caused by turbulence in free-space optical communication. In particular, the Gamma-Gamma (G-G) distribution, a branched stochastic scintillation model, has been shown to agree very well with experimental observations under different channel conditions [3]. The G-G distribution compares very favorably with alternative models such as the Malaga-M (M), Log-Normal (LN), and Fisher-Snedecor (F) distributions for representing atmospheric turbulence in FSO communications. In particular, the G-G model assumes that the signal propagating over the wireless channels is subject to small-scale and large-scale fluctuations, both of which are modeled by the Gamma distribution. The ability of the G-G distribution model to capture a wide range of turbulence (i.e., from weak to strong) is due to its structure, which integrates two separate stochastic variables embodying the small- and large-scale atmospheric. This integration provides a refined and accurate representation of the optical signal's variability as it propagates through the atmosphere [3]. In radio frequency (RF) wireless communications,

Manuscript received 20 May 2024; revised 14 June 2024; accepted 20 June 2024. Date of publication 24 June 2024; date of current version 2 July 2024. (Corresponding author: Wafaa M. R. Shakir)

Wafaa M. R. Shakir and Ali S. Mahdi are with the Computer Systems Department, Technical Institute of Babylon, Technical Al-Furat Al-Awsat Technical University, Babil 51015, Iraq (e-mail: inb.wfaa@atu.edu.iq; ali.khafaja@atu.edu.iq).

Hani Hamdan is with the CentraleSupélec, CNRS, Laboratoire des Signaux et Systèmes (L2S UMR CNRS 8506), Université Paris-Saclay, 91190 Paris, France (e-mail: hani.hamdan@centralesupelec.fr).

Jinan Charafeddine is with Léonard de Vinci Pôle Universitaire, Research Center, 92916 Paris La Défense, France (e-mail: jinan.charafeddine@devinci.fr).

Haitham Al Satai and Radouane Akrache are with the Pôle scientifique et technologique de Vélizy, Laboratoire d'Ingénierie des Systèmes de Versailles (LISVEA4048), Université Paris-Saclay, 78140 Paris, France (e-mail: haitham.al-satai@uvsq.fr; radouane.akrache@uvsq.fr).

Samir Haddad is with the Department of Computer Science and Mathematics, Faculty of Arts and Sciences, University of Balamand, Koura 3936, Lebanon (e-mail: samir.haddad@balamand.edu.lb).

Jinane Sayah is with the Department of Telecom and Networks, Issam Fares Faculty of Technology, University of Balamand, Koura 3936, Lebanon (e-mail: jinane.sayah@balamand.edu.lb).

Digital Object Identifier 10.1109/JPHOT.2024.3418371

user terminals with low mobility are subject to the simultaneous effects of small-scale fading (multipath) and large-scale fading (shadowing), resulting in what is known as composite fading. Modeling multipath fading by the Nakagami- $m$  distribution and shadow fading by the Gamma distribution leads to the G-G model for composite fading [4]. The G-G received power model encompasses the  $K$ -distribution and the Gamma models (which consider either the multipath component or the shadowing individually) as special cases. It also approximates the widely-used Nakagami-lognormal composite fading model. In addition, the G-G model incorporates and generalizes several other turbulence models, including the negative exponential (NE) distribution, the generalized  $K$  distribution ( $K_G$ ) (also called the G-G fading model [5]), the  $I - K$  and the Rice/Nakagami- $m$  distributions. It should also be emphasized that the G-G distribution does not have an exact relationship with the Malaga-M distribution, which means that G-G is an approximate case of the Malaga-M distribution [4].

While the G-G channel model provides a simple analytical approach for analyzing single input single output (SISO) wireless systems, its application to multiple input multiple output (MIMO) systems becomes complex as the collective distribution of the independent G-G variables must be determined.

In addition to fading caused by turbulence, the effectiveness of FSO communications can be significantly affected by pointing errors due to building sway. FSO systems, typically mounted on the tops of tall buildings to maintain line of sight, are susceptible to interference from various elements, such as atmospheric turbulence and the swaying and vibration of buildings due to wind and thermal effects. Pointing errors occur in the form of both boresights (i.e., a static misalignment between the center of the beam and the center of the detector) and jitter, which is a random fluctuation in alignment. Although the installations of terrestrial FSO systems are designed to minimize misalignment, significant deviations can still occur due to the thermal expansion of the building [6], [7]. It is mentioned in [8] that the thermal expansion of buildings can lead to a boresight of up to 0.3 milliradians. In satellite-to-ground and satellite-to-satellite communications, the transmitter and receiver have a high relative velocity, and there is mechanical noise due to satellite motion and gimbal friction [6]. Therefore, it is difficult to realize perfect tracking, and jitter and boresight can also occur as residual pointing errors. The zero-boresight pointing error (ZBPE) model developed in [9] is widely used in the literature [10], [11], [12], [13]. In this model, the boresight component of pointing error is assumed to be zero, and both horizontal and elevation displacements are assumed to follow an independent, identically distributed (i.i.d) zero-mean Gaussian distribution. As a result, the random radial displacement at the receiver is Rayleigh distributed [6]. To account for the difficulties caused by factors such as the width of the optical beam, the size of the detector, the variance of the jitter in different axes, and the existence of non-zero boresight pointing errors (NZBPE), a more detailed and accurate model for characterizing pointing errors has been introduced in the literature [6]. The effect of NZBPE is studied in the literature for terrestrial SISO FSO links [6], [14] and also for mixed radio frequency/free-space optical (RF/FSO) relay systems in the existing literature [15], [16]. The mixed communication system

using both RF and FSO technologies is proposed to utilize the robustness of RF links and the high bandwidth of FSO links. In addition, RF links offer low-cost communication capabilities without line-of-sight, while FSO links offer low transmission latency and extremely high transmission rates. Upadhyaya et al. [15] show that the considered mixed RF/FSO system's overall performance strongly depends on the FSO link model's parameters, especially the pointing error parameter. While in [16], the authors investigate the effect of in-phase/quadrature-phase imbalance on an asymmetric mixed RF/FSO two-way relay (TWR) communication system with multiple co-channel interferers at the relay node in the presence of atmospheric turbulence with NZBPE on the FSO link.

In addition, atmospheric attenuation refers to the reduction in the strength of electromagnetic wave energy as it passes through the atmosphere. This phenomenon results in signal weakening and attenuation in FSO system links through a combination of absorption, scattering, and scintillation, all of which are transient and dependent on the prevailing local environment [17]. In addition, weather conditions, especially fog, smoke, and dust, also result in scattering and attenuation. For example, in a dense fog condition (defined by atmospheric visibility ( $V$ )  $<$  0.5 km), the FSO link failure is high due to the scattering and absorption of the propagating optical beam, which is not desirable by the end users [18].

Techniques such as aperture averaging, adaptive optics, and spatial diversity are invaluable for improving the robustness of FSO communication systems. Implementing MIMO configurations with multiple transmitters and receivers that ensure statistically uncorrelated fading channels can significantly counteract the impairments caused by scattering, turbulence, and misalignment. The effectiveness of this approach has been confirmed in theoretical models and practical experiments [19].

#### A. Related Work

There are numerous studies in the literature on the use of MIMO technology to improve transmission quality and overcome challenges such as atmospheric turbulence, misalignment issues, and adverse weather conditions in FSO communications. Specifically, the research described in [20] investigated different modulation strategies for dual-receive aperture systems navigating through G-G distributed atmospheric turbulence to overcome turbulence-induced transmission degradation. In another study [21], an intensity-modulation/direct detection (IM/DD) approach with equal gain combining (EGC) and maximum ratio combining (MRC) techniques was used in analyzing a MIMO FSO communication system. This research focused on a channel characterized by G-G turbulence and addressed the stability issues at high signal-to-noise ratios (SNR) using a generalized infinite power series. A further investigation of the relationship between bit error rate (BER) and SNR for a MIMO FSO system using repetitive and Alamouti coding in a distributed G-G turbulence environment was documented in [22]. It is important to note that these studies used an infinite power series expansion of a Bessel function term to derive the probability density function (PDF) approximation for the G-G turbulence channels [20], [21], [22].

Further elaborating in [23], the study has addressed the BER of binary phase shift keyed (BPSK) modulation schemes for single input multiple outputs (SIMO) FSO communication under a negative exponential turbulence channel. This research provides additional perspectives on how modulation techniques can serve as countermeasures against the effects of channel impairments. The benefits of using multiple receiver apertures together with combination strategies such as selection combining (SC), EGC, and MRC were highlighted. The results show that MRC performs better than EGC and SC, especially in environments affected by non-Gaussian noise and additive white Gaussian noise (AWGN).

Moreover, the authors in [24] investigated the effectiveness of M-ary PSK (MPSK) modulation within MIMO FSO communications considering the Malaga-M atmospheric turbulence channel. The results of this study show a significant decrease in the average BER, which correlates with an increase in the number of transmit and receive apertures. It is essential to recognize that the initial research on MIMO FSO systems did not consider the effects of pointing errors or disparity due to atmospheric attenuation [20], [21], [22], [23], [24]. Furthermore, in [25], the synergistic influence of G-G distributed atmospheric turbulence combined with attenuation factors such as drizzle, haze, and fog on FSO communications with multiple receivers was investigated, and it was found that increasing the number of receivers led to a decrease in BER. Further progress in [25], [26] focused on extending the study to MIMO FSO links, incorporating both attenuation and G-G distributed turbulence to evaluate the BER [25] and the outage probability ( $P_{out}$ ) [26] of the systems. The study in [27] integrated the effects of Gaussian-distributed ZBPE (GZBPE) and NE-distributed turbulence-induced fading. This study focused on the outage performance of a horizontal MIMO FSO link using the intensity modulation and direct detection (IM/DD) scheme. The results show that the reliability is significantly improved by using EGC. Studies in [28] investigated the influence of ZBPE and G-G turbulence on the efficiency of on-off keying (OOK) modulated FSO systems with multiple receiver apertures. In addition, log-normal fading channel models were also considered [29]. It is noteworthy that the mathematical representation of the MIMO FSO channel in the [23], [24], [25], [26], [27], [28], [29] studies was limited to analyzing the effect of diversity techniques on the SNR of the systems. Similarly, the study in [30] investigated the performance of an FSO system with a SIMO diversity scheme in a horizontal configuration under the cumulative effects of attenuation, ZBPE modeled by the Rayleigh distribution, and G-G turbulence. In addition, the effectiveness of a SIMO FSO links with PSK modulation on subcarriers was investigated in [31], considering the cumulative effects of G-G distributed turbulence, attenuation, and Rayleigh distributed pointing errors.

Given the challenges and computational limitations of deriving exact PDFs for FSO communications in optical MIMO configurations, the search for approximate distribution models has been pursued. A first method was proposed in [32] to approximate the PDF of the sum of independent and not necessarily identically distributed (i.n.i.d) G-G random variables by another G-G distribution using a refined version of the

moment-matching technique. In this approach, the parameters of the approximated G-G PDF were adjusted by minimizing the numerical discrepancy between the estimated and actual PDFs. The authors extended their work to include RF systems [33] rather than focusing on wireless optical communications [32]. It is worth noting that the closed-form PDF expressions for the sum of G-G variates that efficiently approximated in [32] have been widely utilized in both wireless optical [34] and RF systems for analyzing either the common end-to-end communication performance or evaluating the secrecy performance of diversity receiver systems in terms of average secrecy capacity (ASC), security outage probability (SOP), and the probability of strictly positive secrecy capacity (SPSC) [35], [36].

However, these approximations were less precise for minimal fading parameter values and the case of independent and not identically distributed (i.n.d.) variables. Subsequently, the researchers in [34] extended the method from [32] for MIMO FSO communications by approximating the sum of i.i.d. G-G turbulence in combination with Rayleigh-distributed ZBPE to analyze both the BER and ergodic capacity ( $C$ ) of MIMO FSO links. However, it was found that a lower approximation accuracy was achieved, especially in scenarios with strong pointing error effects. The authors in [37] also used moment matching to develop an approximate  $\alpha - \mu$  PDF for the aggregate of i.i.d. G-G variables. At the same time, an approximation for the sum of Malaga-M variables with Rayleigh ZBPE was investigated in [38] using an approximation with Fox's H-function derived from the moment-generating function (MGF) technique. The accuracy of this model was found to be lower, especially for smaller moment values. In another related research work [39], a performance analysis of MIMO FSO links using the EGC technique was presented, assuming a combined lognormal-Rician for atmospheric turbulence with Rayleigh ZBPE. An analytical approximation for the sum distribution of MIMO channels was introduced using a series representation for identically distributed lognormal-Rician variables. This approximation also showed limited accuracy, particularly for a large number of transmit and receive apertures or for small values of pointing errors. Finally, several studies have investigated different aspects of diversity techniques for FSO systems, including EGC reception for SIMO FSO over an independent and not necessarily identically distributed channel fading modeled by the mixture-Gamma (M-G) distribution [40] and spatial diversity for mixed user-diversity RF and spatial diversity FSO cooperative relaying systems [41]. The M-G distribution was chosen because it can effectively approximate both the G-G and Malaga-M distribution models and provides accurate modeling under weak to strong turbulence conditions. Similar work investigating the performance of mixed RF/FSO relay systems with different diversity techniques can be found in [42] and [43].

A review of recent and relevant studies reveals several research gaps for FSO communications in MIMO environments that must be addressed. First, the analyses have either overlooked the loss due to pointing errors or limited their scope to zero bore-sight in MIMO FSO transmission systems. The non-zero bore-sight pointing errors model extends the understanding of these effects of misalignment on FSO transmission. It is important to



mention here that the statistical analysis of NZBPE with generalized Rician distribution remains unexplored due to the complexity involved in analyzing such a model within the context of a MIMO FSO environment. Secondly, signal attenuation in FSO transmissions is usually considered deterministic and depends on visibility conditions. For example, attenuation is lower in clear skies, and signal power loss is greater in fog [1]. Similar to the NZBPE loss, atmospheric attenuation was not included in the MIMO FSO analyses. Our work considers a deterministic atmospheric loss model to account for signal attenuation in MIMO FSO transmissions [44]. Thirdly, the G-G distribution has been the preferred model for atmospheric conditions ranging from weak to strong turbulence. While the use of the G-G distribution to describe atmospheric turbulence in SISO-FSO transmission has been extensively studied [45], [46], its application in a MIMO-FSO context introduces significant complexity. This is due to the existence of the modified Bessel function of the second kind, which complicates a precise statistical analysis of MIMO-FSO systems.

### B. Motivation and Contributions

MIMO FSO systems are renowned for their ability to counteract turbulence-induced fading and enhance performance significantly. However, as far as we know, very few works address terrestrial MIMO FSO communication systems under realistic channel conditions. Most existing systems overlook the impact of non-zero boresight pointing errors and atmospheric loss, which considerably degrade such communication systems' performance. Unlike many previous works that employ an unrealistic zero boresight pointing error model—suitable for SISO but inadequate for MIMO FSO systems—our work pioneers a more practical approach tailored for MIMO FSO transmission. This represents a substantial advancement in the field. Even in the aforementioned works that propose the structure of the pointing error model suitable for MIMO transmissions, only the ZBPE model with Rayleigh distribution [34] is considered, which only takes the jitter loss into account. We propose a comprehensive statistical model that includes both jitter and boresight effects, using a sum of Rician-distributed variates to model the pointing error losses across MIMO links. We have developed a novel closed-form probability density function for our comprehensive pointing error model using a series representation for the  $\kappa - \mu$  distribution. Then, we developed a new model that takes into account the aggregate effects of the sum of G-G random variates, generalized NZBPE, and atmospheric attenuation, providing a holistic description of MIMO FSO transmission. Table I summarizes the latest research results in this field.

Using multiple transmitters and receivers between the source and the destination with a wide range of parameters, the main contributions of this work can be briefly summarized as follows:

- 1) For the first time, to the best of the authors' knowledge, our study incorporates the joint impact of atmospheric turbulence, generalized pointing errors, and attenuation in MIMO FSO communication systems.
- 2) Using a novel series representation, we introduce a new analytical approximation expression for the sum of the

random variates of Rician non-zero boresight pointing for MIMO FSO transmission.

- 3) The accuracy of this approximation is then validated by statistical tests, including the Kolmogorov-Smirnov (KS) goodness of fit.
- 4) From this approximation, analytical expressions for the PDF and the cumulative distribution function (CDF) of the SNR are obtained using Meijer's G-function.
- 5) Subsequently, we derive expressions for the ergodic capacity, outage probability, and the average BER for the OOK modulation scheme of an FSO link utilizing the EGC technique. All these expressions are presented in terms of Meijer's G function. In addition, the results of the considered MIMO FSO system are compared with the SISO [6] and [14], SIMO [47], and multiple inputs single outputs (MISO) [48] systems.
- 6) In the high SNR region, these are expressed by simple elementary functions that facilitate analysis of the effects of the channel parameters. We also determine the coding gain and diversity order from the asymptotic behavior.
- 7) To verify the accuracy of the newly proposed results, we perform numerical and computational Monte-Carlo simulations. It is noteworthy that a perfect agreement between the analytical expressions and the simulation results can be observed.

The remainder of this paper is structured accordingly: Section II describes the system and channel models in focus. Section III provides the closed-form approximations for the PDF of the sum of G-G variates with NZBPE and atmospheric attenuation. Section IV derives the key performance metrics for the MIMO FSO systems, and Section V showcases numerical simulations that corroborate the analytical findings. Section VI offers concluding thoughts.

## II. SYSTEM AND CHANNEL MODEL

We consider an FSO system with an intensity modulation and direct detection technique equipped with  $M$  transmitters and  $N$  receivers. In such systems, the OOK symbol  $x$  is transmitted simultaneously by all transmitters within each transmission interval. To ensure statistical independence and uncorrelated fading, the transmitters and receivers are positioned at a distance from each other that exceeds the coherence length, typically by several centimeters, since the coherence length itself is of the order of centimeters [49]. The EGC diversity technique is utilized at the receivers, which is an easy-to-implement solution while delivering a performance that is nearly equivalent to optimal combining methods.

The resulting signal of the EGC receiver is then formulated as follows

$$y = \eta \sum_{i=1}^M \sum_{j=1}^N I_{ij} x + \sum_{j=1}^N v_j \quad (1)$$

where  $\eta$  is the optical-to-electrical conversion coefficient,  $v_j$  is additive white Gaussian noise with zero means, and a variance of  $\sigma^2 = N_0/2$ .  $I_{ij}$  denotes the fading channel coefficient between the  $i$ th ( $i = 1, 2, \dots, M$ ) transmitter and the  $j$ th ( $j =$

TABLE I  
RELATED LITERATURE ON THE CHANNEL APPROXIMATION APPROACHES FOR THE DIVERSITY SYSTEMS

Reference	Turbulence model	Pointing errors loss	Attenuation loss	Metrics	Objective	Channel approximation approach
[20]-[22]	G-G	✗	✗	BER	Investigation of the effects of using MIMO technology to mitigate the transmission impairments of the turbulence channel.	Using an infinite power series expansion to represent the Bessel function term to approximate the PDF for the G-G turbulence channels.
[23]	NE	✗	✗	BER	Comparison of the performance of different diversity combining techniques of the SIMO FSO over the NE turbulence channel and optimization of the beam alignment for improving the stability of the system.	Considering the impact of the spatial diversity technique on the SNR of the SIMO system.
[24]	Malaga-M	✗	✗	BER	Investigate the effects of adaptive subcarrier modulation and MIMO techniques on the atmospheric fading channel.	Reflect on the impact of diversity techniques on the SNR of MIMO systems.
[25], [26], [28]	G-G	GZBPE [18]	[25], [26]	BER, $P_{out}$	Evaluation of the effects of turbulence and different weather conditions [25], [26] and the effect of GZBPE [28] on the reliability and efficiency of diversity systems.	Analyzing the diversity combining technique influences the SNR of the diversity systems.
[27]	NE	GZBPE	✗	$P_{out}$	Analyzing the reliability of the MIMO system under conditions of strong turbulence and misalignment fading.	Investigating how diversity combining techniques affect the SNR of the overall MIMO system.
[29]	LN	ZBPE	✗	BER, $P_{out}$	Analyzing the combined effect of channel conditions on the SIMO system with a subcarrier intensity modulation scheme.	Evaluation of the influence of the diversity combining technique on the SNR of the SIMO system.
[30], [31]	G-G	ZBPE	√	BER, $P_{out}$	Quantifying the joint influence of atmospheric turbulence, pointing errors and attenuation losses on SIMO system performance.	Consideration of the effects of the diversity combining technique on the SNR of the SIMO system.
[32], [33]	G-G	✗	✗	BER, $P_{out}$	Investigate the performance of wireless optical [32] and RF [33] wireless over MIMO links.	Approximate the sum of i.n.i distributed G-G variate using the MGF.
[34]	G-G	ZBPE	✗	BER, $C$	Investigate the performance of MIMO FSO system over G-G fading channels with Rayleigh pointing errors.	Approximate the sum of G-G with ZBPE random variates using the series representation for the Rayleigh pointing error.
[35], [36]	$K_G$	✗	✗	SPSC, SOP, ASC	Investigate the security performance of the SIMO RF system over $K_G$ fading channels, considering the impact of various parameters such as antenna number and fading factors.	Approximate the independent $K_G$ distribution by the sum of G-G variates [35] and Gamma and M-G [36] distributions.
[37]	G-G	✗	✗	BER, $P_{out}$	Develop the performance metrics of the MIMO FSO system over the turbulence channel.	Approximate the sum of i.i.d. G-G random variables using the MGF.
[38]	Malaga-M	ZBPE	✗	BER	Evaluate the performance of SIMO FSO transmission over the Malaga-M turbulence channel.	Approximate the PDF of the sum of Malaga-M random variables using the MGF.
[39]	lognormal-Rician	ZBPE	✗	BER, $C$ , $P_{out}$	Evaluate the performance of the MIMO FSO system in lognormal-Rician turbulence with Rayleigh pointing errors.	Approximate the distribution of the sum of the lognormal-Rician turbulence variates with Rayleigh pointing error using a series representation.
[40]	M-G	ZBPE	✗	BER, $P_{out}$	Evaluate the performance of EGC reception in a SIMO FSO system under M-G fading and pointing errors.	A finite-sum series representation of Meijer's G-function is used to approximate the diversity channel representation.
[41]	M-G	ZBPE	✗	BER, $P_{out}$	Analyze the performance of mixed RF user diversity and spatial diversity FSO relay systems with cooperative transmission over an $\alpha$ - $\mu$ /M-G fading channel.	Approximate the diversity of optical links using a finite sum series representation based on the approach introduced in [40].
[42], [43]	G-G	ZBPE [43]	✗	BER, $P_{out}$ , $C$ [43]	Analyze the performance of mixed RF/MIMO FSO relay systems over Nakagami-m [42], $K_G$ [43] for RF links, and G-G for FSO links.	Approximate the sum of the G-G variate of optical links based on the approach introduced in [32].
[This paper]	G-G	Rician NZBPE	√	BER, $C$ , $P_{out}$	Investigate the performance of the RMIMO FSO system over the sum of G-G variates with Rician NZBPE and atmospheric loss channel.	Approximate the distribution of the sum of G-G with NZBPE random variates and atmospheric attenuation for MIMO FSO transmission using a new series representation.

1, 2, ..., N) receiver and is subject to the combined effects of atmospheric loss, turbulence-induced irradiance fluctuation and generalized pointing errors. From (1), the electrical SNR of the combined signal is given by

$$\gamma_{EGC} = \frac{\eta^2 \mathbb{E}[|x|^2] \left( \sum_{i=1}^M \sum_{j=1}^N I_{ij} \right)^2}{N\sigma^2} = \frac{\gamma_0 I^2}{N} \quad (2)$$

where  $\gamma_0 = \eta^2 \mathbb{E}[|x|^2]/\sigma^2$  denotes the average SNR and  $I = \sum_{i=1}^M \sum_{j=1}^N I_{i,j}$ , where  $\mathbb{E}[\cdot]$  represents the expected value. From (2), it can be seen that  $I$  is the key parameter to evaluate the performance metric of error probability of the MIMO FSO system using the EGC diversity technique.

The irradiance  $I$  is considered as the product of the loss due to atmosphere  $I^a$ , the scintillation due to atmospheric turbulence  $I^t$ , and pointing errors  $I^p$ , i.e.,  $I = I^a I^t I^p$ .

Conventionally, the atmospheric loss is modeled by Beers-Lambert law is given as [44]

$$I^a = e^{-\sigma z} \quad (3)$$

where  $\sigma$  denotes the weather-dependent attenuation coefficient, and  $z$  is the FSO link distance between the transmitter and receiver.

Moreover, it has been shown in [50] and [51] that the correlation time of the misalignment caused by the swaying of buildings is in the order of a few seconds, which is more significant than that of atmospheric turbulence, which ranges from 10 to 100 milliseconds. Therefore, the atmospheric turbulence and the misalignment can be considered independent, while  $I^a$  is conventionally considered a constant [6].

To evaluate the behavior of the fading parameter  $I^t$  in different turbulence scenarios, the Gamma-Gamma distribution model is used in this study. The mathematical expression for the probability density function of  $I^t$  is defined as [3]

$$f_{I^t}(I^t) = \frac{2(\alpha\beta)^{\frac{\alpha+\beta}{2}}}{\Gamma(\alpha)\Gamma(\beta)} (I^t)^{(\alpha+\beta)/2-1} K_{\alpha-\beta} \left( 2\sqrt{\alpha\beta I^t} \right), \quad I^t \geq 0 \quad (4)$$

where  $\alpha \geq 0$  and  $\beta \geq 0$  are the shaping parameters that can be directly associated with the strength of the atmospheric turbulence, which is defined by the Rytov variance  $\sigma_z^2$ . The Rytov variance  $\sigma_z^2 = 1.23 C_n^2 k^{7/6} z^{11/6}$ ,  $k = 2\pi/\lambda$  is the optical wave number,  $\lambda$  is the wavelength of propagation, and  $C_n^2$  represents the refractive index structure parameter, which is a quantitative measure of optical turbulence [3].  $\Gamma(\cdot)$  is the Gamma function, and  $K_v(\cdot)$  is the modified Bessel function of the second kind and order  $v$ .

Another performance-limiting factor in FSO communication is the pointing errors caused by misalignment between the transmitter and receiver. When a Gaussian beam propagates through distance  $z$  from the transmitter to a circular detector with aperture radius  $R_a$  and the instantaneous radial displacement between the beam centroid and the detector center,  $r$ , the fraction of the collected power at the receiver can be approximately calculated as follows [6]

$$u(r) = I^p(r) \approx A_0 \exp\left(-\frac{2r^2}{w_{zeq}^2}\right), \quad r \geq 0 \quad (5)$$

where  $A_0 = [erf(v)]^2$  is the fraction of the collected power at  $r = 0$ ,  $v = \sqrt{\frac{R_a^2 \pi}{2w_z^2}}$ , is the ratio between the receiver's aperture radius  $R_a$  and the beam waist  $w_z$ , and  $erf(x) = \frac{2}{\sqrt{\pi}} \int_0^x e^{-t^2} dt$  is the error function, while  $w_z$  is the beam waist that can be approximated by  $w_z = \theta z$  with  $\theta$  denoting the transmit divergence angle, and  $w_{zeq} = \sqrt{w_z^2 \sqrt{\pi} erf(v)/2v \exp(-v^2)}$  represents the equivalent beam waist. At the receiver aperture plane, the radial displacement vector can be expressed as  $r = [r_x, r_y]^T$ , where  $r_x$  and  $r_y$ , respectively, denote the displacements located along the horizontal and elevation axes at the detector plane. We consider non-zero boresight pointing errors in addition to the random jitters and model  $r_x$  and  $r_y$  as non-zero mean Gaussian distributed random variables, i.e.,  $r_x \sim \mathcal{N}(\mu_x, \sigma_x^2)$ ,  $r_y \sim \mathcal{N}(\mu_y, \sigma_y^2)$ . Then, the radial displacement,  $r = |r| = \sqrt{r_x^2 + r_y^2}$  follows the Rician distribution with  $\mu_x^2 + \mu_y^2 \neq 0$ ,  $\sigma_x = \sigma_y$  [6]. In terrestrial FSO systems, however, jitter is mainly caused by turbulence and the swaying of buildings. Since the turbulence cells occur randomly in the beam path and the building can sway with equal probability in orthogonal and horizontal directions to the beam path, we have the following:  $\sigma_x^2 = \sigma_y^2 = \sigma_s^2$ .

As a result, the PDF of radial displacement  $r$  with Rician distribution can be defined as [6]

$$f_r(r) = \frac{r}{\sigma_s^2} \exp\left(-\frac{(r^2+s^2)}{2\sigma_s^2}\right) I_0\left(\frac{rs}{\sigma_s^2}\right) \quad (6)$$

where  $s = \sqrt{\mu_x^2 + \mu_y^2}$  is the boresight displacement, and  $I_v(\cdot)$  is the modified Bessel function of the first kind with order  $v$ . From (5) and (6), the PDF of non-zero boresight pointing error with Rician distribution can be expressed as

$$f_{I^p}(I_p) = \frac{\zeta^2 \exp\left(\frac{-s^2}{2\sigma_s^2}\right)}{A_0 \zeta^2} I_p^{\zeta^2-1} I_0\left(\frac{s}{\sigma_s^2} \sqrt{\frac{-w_{zeq}^2 \ln \frac{I_p}{A_0}}{2}}\right), \quad 0 \leq I_p \leq A_0 \quad (7)$$

Here  $\zeta = w_{zeq}/2\sigma_s$  is the ratio between the equivalent beamwidth and jitter standard deviation, providing a quantitative assessment of the impact of pointing errors. When the boresight error is zero, with  $s = 0$ , the pointing error model expressed in (7) simplifies to the form presented in (5).

### III. AN EFFICIENT APPROXIMATE DISTRIBUTION FOR THE SUM OF GAMMA-GAMMA WITH NZBPE TO MODEL MIMO FSO CHANNEL

In this section, we propose a new distribution approximation for the sum of  $L$  Gamma-Gamma fading with generalized Rician non-zero boresight pointing error random variables and atmospheric loss. Let us consider  $L$  statistically independent  $I$  random variables denoted by  $\{I_l\}_{l=1}^L$ . Their summation is defined as

$$T = \{I_l\}_{l=1}^L = \sum_{l=1}^L x_l u(r_l) \quad (8)$$

where  $x_l$  and  $r_l$  are the Gamma–Gamma and Rician random variables, respectively. Note that (8) can be rewritten as

$$T = \frac{\sum_{l=1}^L x_l \sum_{l=1}^L u(r_l)}{L} + \frac{1}{L} \sum_{i=1}^{L-1} \sum_{j=i+1}^L (x_i - x_j) \times (u(r_i) - u(r_j)) \quad (9)$$

For simplicity, it is assumed that the variables of the sum in (9) are independent and identically distributed random variables. Therefore,  $\{x_l\}_{l=1}^L$  and  $\{u(r_l)\}_{l=1}^L$  are also i.i.d. According to (9), the distribution of  $T$  can be approximated by the distribution of the random variable  $\bar{T}$ , which is expressed as

$$T \approx \bar{T} = \frac{\sum_{l=1}^L x_l \sum_{l=1}^L u(r_l)}{L} \quad (10)$$

with the approximation error  $\varepsilon$  given by

$$\varepsilon = \frac{1}{L} \sum_{i=1}^{L-1} \sum_{j=i+1}^L (x_i - x_j) (u(r_i) - u(r_j)) \quad (11)$$

Note that the distribution in (11) can be regarded as the product of two random variables,  $t_1$  and  $t_2$ , i.e.,  $\bar{T} = t_1 t_2$  where  $t_1 = \sum_{l=1}^L x_l$  and  $t_2 = \frac{1}{L} \sum_{l=1}^L u(r_l)$ .

It has been shown that the distribution of the sum of i.i.d. Gamma-Gamma variates ( $k_l = k, m_l = m, \Omega_l = 1$ ) can be efficiently approximated by a G-G distribution with parameters  $a, b, \omega$  [33]. This distribution is defined as

$$f_{t_1}(t_1) = \frac{2(ab)^{\frac{(a+b)}{2}}}{\Gamma(a)\Gamma(b)\omega^{\frac{(a+b)}{2}}} t_1^{\frac{(a+b)}{2}} K_{a-b} \left( 2\sqrt{\frac{ab}{\omega}} t_1 \right) \quad (12)$$

where  $a = Lk + (L-1)\frac{-0.127-0.95k-0.0058m}{1+0.00124k+0.98m}$ ,  $b = Lm$ ,  $\omega = L$  [33].

Next, we will solve the distribution for random variables  $\bar{T}$ , by proposing a new approximate distribution for the sum of variates of generalized non-zero boresight pointing errors for MIMO FSO transmissions.

Note that the squared Rician distribution is a special case of the  $\kappa - \mu$  distribution with  $\kappa = r, \mu = 1, \Omega = 1$  as shown in [52]. Therefore, it is shown by [53] that the sum of  $L$  i.i.d.  $\kappa - \mu$  random variables with parameters  $\kappa = r, \mu, \Omega$  is also a  $\kappa - \mu$  random variable with parameters  $\kappa = r, L\mu, L\Omega$ . Then the PDF of the random variable,  $U = \sum_{l=1}^L u(r_l)$  can be approximated as

$$f_U(r) \approx \frac{L \left(\frac{s}{\sigma_s^2}\right)^{\frac{L+1}{2}} \exp\left(\frac{-Ls^2-r^2}{2\sigma_s^2}\right) u^{L-1}}{\left(\frac{s^2}{2\sigma_s^2}\right)^{\frac{L-1}{2}} L^{\frac{L+1}{2}}} I_{L-1} \left(\frac{Lsr}{\sigma_s^2}\right) \quad (13)$$

The above formula can be rewritten as

$$\begin{aligned} f_U(r) &\approx \sum_{q=0}^Q \frac{\left(\frac{s}{2\sigma_s^2}\right)^q \exp\left(\frac{-Ls^2-r^2}{2\sigma_s^2}\right)}{q! \Gamma(L+q)} \\ &\times \left(\frac{Ls}{2\sigma_s^2}\right)^{L+2q-1} r^{L+2q-1} + R_Q(r) \\ &\approx \sum_{q=0}^Q \frac{2 \left(\frac{s}{2\sigma_s^2}\right)^q \exp\left(\frac{-Ls^2}{2\sigma_s^2}\right) \left(\frac{Ls}{2\sigma_s^2}\right)^{L+2q-1}}{q! \Gamma(L+q)} H_{0,1}^{1,0} \end{aligned}$$

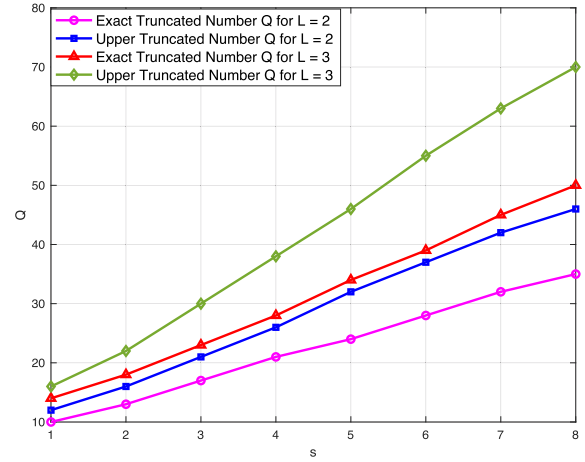


Fig. 1. The smallest truncated number  $Q$  that reaches the maximum error  $\varepsilon = 10^{-5}$ .

$$\times \left[ \frac{r}{2\sigma_s^2} \middle| \begin{matrix} - \\ 2L+q-1, 1 \end{matrix} \right] \quad (14)$$

In (14), we have applied the series expansion result onto the  $I_{L-1}(\cdot)$  [[54], Eq. (8.445)], and expressed the  $\exp(\cdot)$  in terms of the Fox's H function [[55], Eq. (2.5)]. The last equality in (14) holds due to [[55], Eq. (2.4)]. The symbol  $R_Q(r)$  in (14) denotes the truncation error, and is expressed as

$$R_Q(r) = \sum_{q=Q+1}^{\infty} \frac{L \left(\frac{s}{\sigma_s^2}\right)^{L+1} \exp\left(\frac{-Ls-r^2}{2\sigma_s^2}\right)}{q! \Gamma(L+q) \left(\frac{Ls^2}{2\sigma_s^2}\right)^{\frac{L+1}{2}}} \left(\frac{Lsr}{\sigma_s^2}\right)^{L+q} (r)^{L-1} \quad (15)$$

*Theorem 1:* When the truncated number  $Q$  is large enough, the truncation error  $R_Q(r)$ , is upper bounded by

$$R_Q(r) < \frac{\left(\frac{Ls^2}{2\sigma_s^2}\right)^{L+1}}{2\pi Q} \left( \frac{\left(\frac{Ls^2}{2\sigma_s^2}\right) \exp(1)}{(Q+1)} \right)^{Q+1} \quad (16)$$

*Proof:* See Appendix A.

Fig. 1 displays the minimum values of the truncation number  $Q$  required to maintain a maximum error  $\varepsilon$  of  $10^{-5}$  across various scenarios. These values for  $Q$  are calculated based on the truncation error  $R_Q(r)$ , and the upper bound presented in (16). The graph shows that the exact and the upper limits of  $Q$  increase approximately linearly with the parameter  $s$ , converging closely when  $s$  is small. Furthermore, it is determined that setting  $Q$  to 50 is adequate for ensuring the precision of the results across a broad spectrum of channel conditions.

Now, by utilizing [[55], Theorem (4.1)] and the relationship between  $I^p$  and  $u(r)$  of (5) and (7) respectively, the probability distribution for the sum of random variables  $\sum_{l=1}^L u(r_l)$  can be



characterized as

$$\begin{aligned}
 f_{t_2}(t_2) &\approx \sum_{q=0}^Q \frac{\left(\frac{sL}{2\sigma_s^2}\right)^{L+2q+1} \exp\left(\frac{-Ls}{2\sigma_s^2}\right)}{q!\Gamma(L+q)} \\
 &\times \left(\frac{w_d^2 \ln \frac{t_2}{A_0}}{2\sigma_s^2}\right)^{2L+q-1} \exp\left(\frac{-w_d^2 \ln \frac{t_2}{A_0}}{2\sigma_s^2}\right) \\
 &\approx \sum_{q=0}^Q \frac{\left(\frac{sL}{2\sigma_s^2}\right)^{L+2q+1} \exp\left(\frac{-Ls}{2\sigma_s^2}\right) \exp(\zeta^2)}{q!\Gamma(L+q)} \\
 &\times \zeta^{4L+2q-2} \left(\frac{t_2}{A_0}\right) \ln^{2L+q-1} \left(\frac{t_2}{A_0}\right)
 \end{aligned} \quad (17)$$

As a result, the distribution of  $\bar{T}$  is derived through the following

$$\begin{aligned}
 f_{\bar{T}}(t) &= \int_{\frac{t}{A_0}}^{\infty} \frac{1}{t} f_{t_1}\left(\frac{t}{t_1}\right) f_{t_2}(t_1) dt_1 \\
 &= \int_{\frac{t}{A_0}}^{\infty} \frac{\sum_{q=0}^Q \left(\frac{sL}{2\sigma_s^2}\right)^{L+2q+1} \exp\left(\frac{-Ls}{2\sigma_s^2}\right) \exp(\zeta^2)}{q!\Gamma(L+q)} \ln^{2L+q-1} \left(\frac{t}{A_0}\right) \\
 &\times \zeta^{4L+2q-2} \frac{2(ab)^{\frac{a+b}{2}}}{\Gamma(a)\Gamma(b)I^a \omega^{\frac{a+b}{2}}} t_1^{\left(\frac{a+b}{2}\right)-1} K_{a-b} \left(2\sqrt{\frac{ab}{\omega I^a}} t_1\right) dt_1 \\
 &= \frac{\sum_{q=0}^Q 2(ab)^{\frac{a+b}{2}} \left(\frac{sL}{2\sigma_s^2}\right)^{L+2q+1} \exp(\zeta^2) \zeta^{2(2L+q-1)}}{q!\Gamma(a)\Gamma(b)I^a \omega^{\frac{a+b}{2}} A_0^{2L+q-1} \Gamma(L+q)} \\
 &\times \left(\frac{t}{A_0}\right)^{\frac{a+b}{2}-1} \int_1^{\infty} t^{\frac{a+b}{2}-1} \ln^{2L+q-1}(t) K_{a-b} \left(2\sqrt{\frac{abt}{I^a \omega}}\right) dt.
 \end{aligned} \quad (18)$$

The integration of (18) is solved by representing the Bessel function  $K_v(x)$  through Meijer's G-function as specified in [[56], (14)]. By applying the identity given in [[56], (26)], we can establish the following integration formula

$$f(t) = \int_{\frac{t}{A_0}}^{\infty} \frac{1}{y} t^{\frac{a+b}{2}-1} \exp\left(-\frac{abt}{A_0 I^a \omega}\right) \ln^{2L+q-1} \left(\frac{A_0 t}{y}\right) dt \quad (19)$$

Next, to address the above integration, we use the identity provided in [[34], Eq. (79)] as

$$\begin{aligned}
 \int_1^{\infty} x^{v-1} \exp(-tx) \ln^m(x) dx \\
 = \Gamma(m+1) t^{-v} G_{m+1, m+2}^{m+2, 0} \left(t \Big|_{v, 0, \dots, 0}\right)
 \end{aligned} \quad (20)$$

Then, by using (20), we have the following

$$\begin{aligned}
 f_{\bar{T}}(t) &= \frac{\sum_{q=0}^Q 2(ab)^{\frac{a+b}{2}} \left(\frac{sL}{2\sigma_s^2}\right)^{L+2q+1} \Gamma\left(\frac{L+2q+1}{2}\right)}{q! 2^{2L+q-1} \pi \Gamma(a)\Gamma(b) \omega^{\frac{a+b}{2}} A_0 I^a \Gamma(L+q)} \\
 &\times \exp(\zeta^2) \zeta^{4L+2q-2} \left(\frac{ab}{2A_0 I^a \omega}\right)^{\frac{a+b+3}{2}} t^{\frac{L+2q+a+b+4}{2}-1} \\
 &\times G_{L+2q+1, 2L+q+1}^{L+2q+1, 0} \left(\frac{abLt}{2A_0 I^a \omega} \Big|_{\{1\}_{l=1}^L}, \left\{\frac{a+b+3}{2}\right\}, \{0\}_{l=1}^L}\right)
 \end{aligned} \quad (21)$$

Additionally, by leveraging [[56], (26)] in conjunction with [[54], Eq. (9.31.5)], we are able to obtain the cumulative density function for the combined fading channel as

$$\begin{aligned}
 F_{\bar{T}}(t) &= \sum_{q=0}^Q \frac{2(ab)^{\frac{a+b}{2}} \left(\frac{sL}{2\sigma_s^2}\right)^{L+2q+1} \Gamma\left(\frac{L+2q+1}{2}\right)}{q! 2^{2L+q-1} \pi \Gamma(a)\Gamma(b) \omega^{\frac{a+b}{2}} A_0 I^a \Gamma(L+q)} \\
 &\times \exp(\zeta^2) \zeta^{4L+2q-2} \left(\frac{ab}{2A_0 I^a \omega}\right)^{\frac{a+b+3}{2}} \\
 &\times G_{L+2q+2, 2L+q+2}^{L+2q+1, 1}
 \end{aligned}$$

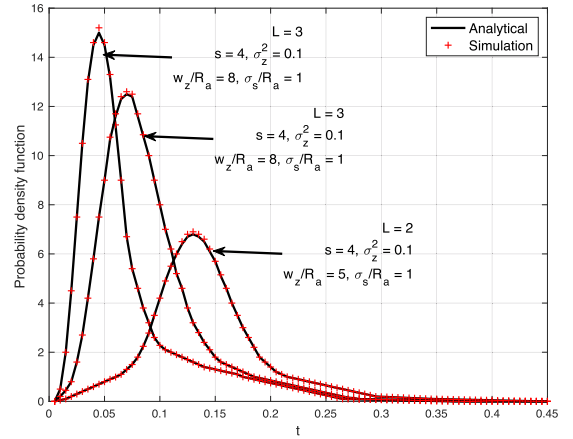


Fig. 2. Comparison between the obtained analytical PDFs and the Monte-Carlo simulations.

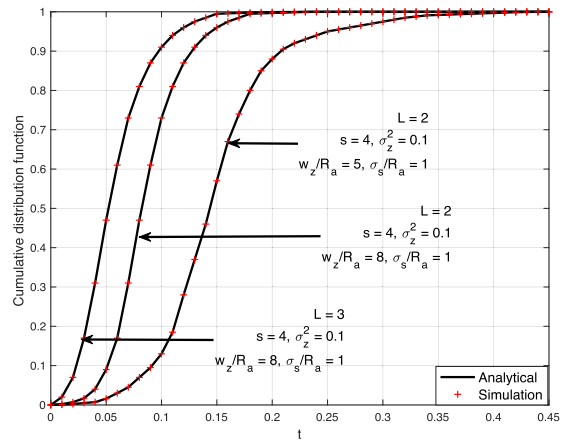


Fig. 3. Comparison between the analytical CDFs and the Monte-Carlo simulations.

$$\left( \frac{abLt}{2A_0 I^a \omega} \Big|_{\left\{1, \left\{\frac{L+2q+a+b+6}{2}\right\}_{l=1}^L\right\}, \left\{\frac{L+2q+a+b+4}{2}\right\}_{l=1}^L}, 0 \right) \quad (22)$$

Figs. 2 and 3 examine the precision of the proposed approximate probability and cumulative density functions by comparing these analytical expressions against the statistical properties derived from simulation data. These comparisons are conducted for varied transmitter and receiver configurations, assuming  $L = MN$ , and incorporating non-zero boresight pointing error effects and turbulence conditions. The simulated PDFs and CDFs, derived from  $10^6$  samples through the Monte-Carlo simulation, serve as the benchmark. The analyses show that the analytical results consistently align closely with the simulation outcomes.

To validate the accuracy of the proposed approximation in (21), the Kolmogorov-Smirnov goodness-of-fit statistical test is applied. This test gauges the most significant absolute discrepancy between the empirical cumulative distribution function of the random variable  $T$ , denoted  $F_T(\cdot)$ , and the approximated  $F_{\bar{T}}(\cdot)$  in (22). Therefore, the KS test statistic is formulated as

$$S = \max |F_T(t) - F_{\bar{T}}(t)| \quad (23)$$



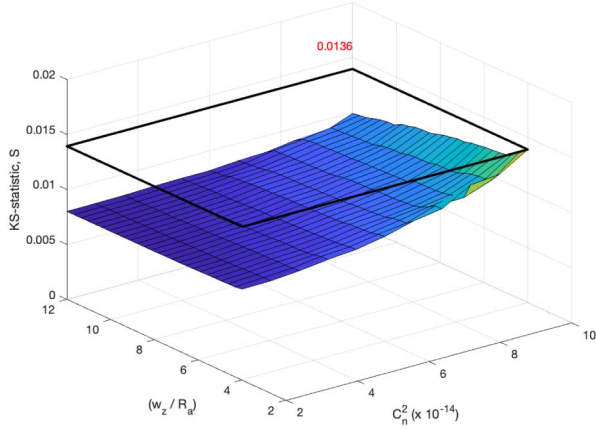


Fig. 4. The KS goodness-of-fit tests with  $\sigma_S/R_a = 2$ ,  $z = 3$  km, and  $L = 3$ .

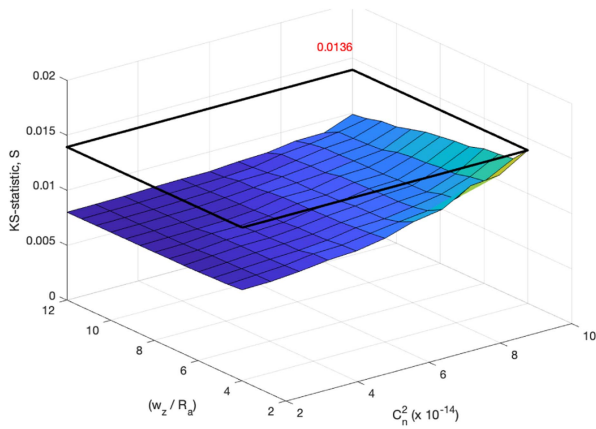


Fig. 5. The KS goodness-of-fit tests, with  $\sigma_S/R_a = 2$ ,  $z = 3$  km, and  $L = 4$ .

According to the findings in [57], an approximation is deemed acceptable at a significance level of  $(1 - \alpha)$  if the KS statistic  $S$  is smaller than a certain critical value  $S_{\max}$ . Conversely, the approximation is rejected at the same significance level if  $S > S_{\max}$ .

The critical value  $S_{\max}$  is determined by  $S_{\max} = \sqrt{-\frac{1}{2K} \ln(\frac{\alpha}{2})}$ , where  $\alpha$  represents the significance level and  $K$  the sample size. Typically, these are set at  $\alpha = 5\%$  and  $K = 10^6$ .

Figs. 4 and 5 illustrate the KS test statistics between the distribution of  $S$  and the approximate distribution in (22) with a 5% significance level for various parameter configurations, such as  $w_z/R_a$ ,  $C_n^2$ , and  $L$ , assuming an i.i.d sum of variates. The data presented are the average outcomes from 100 simulation iterations, each iteration utilizing at least  $10^6$  samples of the random variables. The threshold value  $S_{\max} = 0.0136$  is also provided for reference. Analysis of these figures indicates that the precision of the approximation is significantly influenced by the ratio  $w_z/R_a$  when  $\sigma_S/R_a$  is held constant. Yet, it shows negligible sensitivity to the strength of turbulence.

#### IV. PERFORMANCE ANALYSIS FOR THE MIMO FSO SYSTEMS

This section focuses on analyzing the ergodic capacity, outage probability, and average bit error rate of MIMO FSO systems operating over Gamma-Gamma fading channels, where non-zero boresight pointing errors and atmospheric attenuation are considered, using the presented approximation model.

##### A. Ergodic Capacity Analysis

Under the assumption that the instantaneous channel information is accurately known at the receiver end, the ergodic capacity of the MIMO FSO systems, measured in bits/Hz/s, is determined by the following expression [39]

$$C = \mathbb{E} \left[ \log_2 \left( 1 + \frac{\gamma_0 t^2}{N} \right) \right] \quad (24)$$

A closed-form expression for the ergodic capacity of MIMO FSO communication systems can be obtained as

$$C = \alpha_1 \exp(\zeta^2) \zeta^{4L+2q-2} \left( \frac{abL}{2A_0 I^a \omega} \right)^{-\frac{L+2q+a+b+4}{2}} \times G_{4L+4q+6, 2L+4q+4}^{1, L+2q+3} \left( \frac{4\gamma_0 (A_0 I^a \omega)^2}{N(abL)^2} \middle| \begin{matrix} B_1 \\ B_2 \end{matrix} \right) \quad (25)$$

where

$$A_1 = \frac{\sum_{q=0}^Q 2(ab)^{\frac{a+b}{2}} \left( \frac{sL}{2\sigma_s^2} \right)^{L+2q+1} \Gamma(\frac{L+2q+1}{2})}{q! 2^{2L+q-1} \pi \ln(2) \Gamma(a) \Gamma(b) \omega^{\frac{a+b}{2}} A_0 I^a \Gamma(L+q)},$$

$$B_1 = 1, 1, \left\{ \frac{3-L+2q}{4} \right\}_{l=1}^L, \left\{ \frac{-2-L+2q-a-b}{4} \right\}, \text{ and } B_2 = 1, 0, \left\{ -\frac{4+L+2q+a+b}{4} \right\}_{l=1}^L.$$

*Proof:* See Appendix B.

At higher SNR values, the ergodic capacity reaches an asymptotic expression, which can be depicted by expanding Meijer's G-function using (46) from Appendix B. This expansion allows for a simplified representation of ergodic capacity in terms of basic elementary functions as

$$\bar{C} = A_1 \exp(\zeta^2) \zeta^{4L+2q-2} \left( \frac{abL}{2A_0 I^a \omega} \right)^{-\frac{L+2q+a+b+4}{2}} [6pt] \times \sum_{k=1}^{L+2q+3} \left( \frac{4\gamma_0 (A_0 I^a \omega)^2}{N(abL)^2} \right)^{B_{1k}-1} \times \frac{\prod_{i=1, i \neq k}^{L+2q+3} \Gamma(B_{1k} - B_{1i}) \Gamma(1 + B_{2i} - B_{1k})}{\prod_{i=2}^{4L+4q+6} \Gamma(1 + B_{1i} - B_{1k}) \prod_{i=2}^{2L+4q+4} \Gamma(B_{1k} - B_{2i})} \quad (26)$$

where  $B_{uv}$  represents the  $v^{th}$  term of  $B_u$ .

Taking into account this fact and understanding that the influence of pointing errors can be minimized when setting  $A_0 \rightarrow 1$  and  $\zeta \rightarrow \infty$  [48], we subsequently derive the exact and asymptotic expressions for ergodic capacity as depicted in (27) and (28), respectively

$$C_{np} = A_2 \left( \frac{ab}{2I^a \omega} \right)^{-\frac{2q+a+b+4}{2}} G_{4q+6, 4q+4}^{1, 2q+3} \left( \frac{4\gamma_0 I^a \omega^2}{N a^2 b^2} \middle| \begin{matrix} B_3 \\ B_4 \end{matrix} \right) \quad (27)$$

$$\bar{C}_{np} = A_2 \left( \frac{ab}{2I^a \omega} \right)^{-\frac{2q+a+b+4}{2}} \sum_{k=1}^{2q+3} \left( \frac{(I^a \omega)^2}{N(ab)^2} \right)^{A_k-1} \quad (28)$$

$$\times \frac{\prod_{i=1, i \neq k}^{2q+3} \Gamma(A_{1k}-A_{1i}) \Gamma(1+B_{1i}-A_{1k})}{\prod_{i=2}^{4q+6} \Gamma(1+A_{1i}-A_{1k}) \prod_{i=2}^{4q+4} \Gamma(A_{1k}-B_{1i})}$$

Here,  $\alpha_2 = \frac{\sum_{q=0}^Q 2(ab)^{\frac{a+b}{2}} \left( \frac{sL}{2\sigma_s^2} \right)^{2q+1} \Gamma(\frac{2q+1}{2})}{q! 2^{q-1} \pi \ln(2) \Gamma(a) \Gamma(b) A_0 I^a \omega^{\frac{a+b}{2}} \Gamma(q)}$ ,  $B_3 = \{1, 1, \frac{3+2q}{4}, \frac{-2+2q-a-b}{4}\}$ , and  $B_4 = \{1, 0, -\frac{4+2q+a+b}{4}\}$ .

### B. Outage Probability

Outage probability is a crucial metric for evaluating performance, defined as the probability that the system's instantaneous combined SNR, denoted by  $\gamma_{EGC}$ , falls below a predetermined threshold  $\gamma_{th}$ . Mathematically, the outage probability can be expressed as [39]

$$P_{out} = \Pr(\gamma_{EGC} < \gamma_{th}) = \int_0^{\sqrt{\frac{N\gamma_{th}}{\gamma_0}}} f_{\bar{T}}(t) dt \quad (29)$$

The outage performance for MIMO FSO systems is as follows

$$P_{out} = \alpha_3 \exp(\zeta^2) \zeta^{4L+2q-2} \left( \frac{ab}{2A_0 I^a \omega} \right)^{\frac{a+b+3}{2}} \times G_{L+2q+2, 2L+q+2}^{L+2q+1, 1} \left( \frac{abL \sqrt{\frac{N\gamma_{th}}{\gamma_0}}}{2A_0 I^a \omega} \right)_{B_6}^{B_5} \quad (30)$$

In (30),  $\alpha_3 = \frac{\sum_{q=0}^Q 2(ab)^{\frac{a+b}{2}} \left( \frac{sL}{2\sigma_s^2} \right)^{L+2q+1} \Gamma(\frac{L+2q+1}{2})}{q! 2^{2L+q-1} \pi \Gamma(a) \Gamma(b) \omega^{\frac{a+b}{2}} A_0 I^a \Gamma(L+q)}$ ,  $B_5 = 1, \{\frac{L+2q+a+b+6}{2}\}_{l=1}^L$ , and  $B_6 = \{\frac{L+2q+2a+2b+7}{2}\}_{l=1}^L, 0$ .

*Proof:* See Appendix C.

Furthermore, an asymptotic closed-form expression for the outage probability is given by

$$\bar{P}_{out} = \alpha_3 \exp(\zeta^2) \zeta^{4L+2q-2} \left( \frac{ab}{2A_0 I^a \omega} \right)^{\frac{a+b+3}{2}} \times \sum_{k=1}^{L+2q+1} \left( \frac{abL \sqrt{\frac{N\gamma_{th}}{\gamma_0}}}{2A_0 I^a \omega} \right)^{-B_{5k}} \times \frac{\prod_{i=1, i \neq k}^{L+2q} \Gamma(B_{5k}-B_{5i}) \Gamma(1+B_{6i}-B_{5k})}{\prod_{i=2}^{2L+q+2} \Gamma(1+B_{5i}-B_{5k}) \Gamma(B_{5k}-B_{6i})} \quad (31)$$

### C. Average BER Performance

For a MIMO FSO system employing OOK modulation, the average BER performance is given by [21]

$$P_b = \mathbb{E} \left[ \frac{1}{2} \operatorname{erfc} \left( \sqrt{\frac{\gamma_0 t^2}{4N}} \right) \right] \quad (32)$$

The closed-form expression for the average BER of MIMO FSO communication systems can be obtained as

$$P_b = \alpha_4 \exp(\zeta^2) \zeta^{4L+2q-2} \left( \frac{abL}{2A_0 I^a \omega} \right)^{-\frac{L+2q+a+b+4}{2}}$$

$$\times G_{4L+4q+6, 2L+4q+4}^{L+2q+3} \left( \frac{4\gamma_0 (A_0 I^a \omega)^2}{(abL)^2} \right)_{B_8}^{B_7} \quad (33)$$

where

$$\alpha_4 = \frac{\sum_{q=0}^Q 2(ab)^{\frac{a+b}{2}} \left( \frac{sL}{2\sigma_s^2} \right)^{L+2q+1} \Gamma(\frac{L+2q+1}{2})}{q! 2^{2L+q+1} \pi^{\frac{3}{2}} \ln(2) \Gamma(a) \Gamma(b) \omega^{\frac{a+b}{2}} A_0 I^a \Gamma(L+q)}$$

$$B_7 = 1, \left\{ -\frac{L+2q-2a-2b+3}{4} \right\}, \left\{ -\frac{a+b+1}{4} \right\}_{l=1}^L, \quad \text{and} \quad B_8 = 1, 0.5, \left\{ -\frac{L+2q+a+b-4}{4} \right\}_{l=1}^L.$$

*Proof:* See Appendix D.

Asymptotically, at high SNR, the average BER can be expressed as

$$\bar{P}_b = \alpha_4 \exp(\zeta^2) \zeta^{4L+2q-2} \left( \frac{abL}{2A_0 I^a \omega} \right)^{-\frac{L+2q+a+b+4}{2}} \times \sum_{k=1}^{L+2q+3} \left( \frac{4\gamma_0 (A_0 I^a \omega)^2}{(abL)^2} \right)^{-B_{7k}} \times \frac{\prod_{i=1, i \neq k}^{L+2q+3} \Gamma(B_{7k}-B_{7i}) \Gamma(1+B_{8i}-B_{8k})}{\prod_{i=2}^{2L+q+2} \Gamma(1+B_{8i}-B_{8k}) \prod_{i=2}^{2L+4q+4} \Gamma(B_{7k}-B_{8i})} \quad (34)$$

Additionally, utilizing  $\bar{P}_b \approx (G_c \gamma_0)^{-G_d}$  [[58], (1)], we can easily share that the coding gain  $G_c$  is given as

$$G_c = \frac{4(A_0 I^a \omega)^2}{(abL)^2} \left( \alpha_4 \exp(\zeta^2) \zeta^{4L+2q-2} \left( \frac{abL}{2A_0 I^a \omega} \right)^{-\frac{L+2q+a+b+4}{2}} \times \frac{\prod_{i=1, i \neq k}^{L+2q+3} \Gamma(B_{7k}-B_{7i}) \Gamma(1+B_{8i}-B_{8k})}{\prod_{i=2}^{2L+q+2} \Gamma(1+B_{8i}-B_{8k}) \prod_{i=2}^{2L+4q+4} \Gamma(B_{7k}-B_{8i})} \right)^{-\frac{1}{B_{7k}}} \quad (35)$$

Thus, the diversity order  $G_d$  is given as

$$G_d = \min \left\{ \frac{L+2q-2a-2b+3}{4}, \frac{a+b+1}{4} \right\} \quad (36)$$

## V. NUMERICAL RESULTS AND DISCUSSION

This section shows a numerical analysis of the ergodic capacity, outage probability, and average bit error rate of MIMO FSO systems. These systems are investigated under the influence of generalized atmospheric turbulence, non-zero pointing errors, and atmospheric attenuation. The Monte-Carlo simulations performed in MATLAB serve as a reference point for all figures. We outline the Monte-Carlo simulation process as follows: Using the specified channel parameters  $\gamma_0$ ,  $M$ ,  $N$ ,  $\sigma_z^2$ ,  $w_z/R_a$ ,  $\sigma_s/R_a$ , we synthesize  $10^6$  independent and identically distributed Gamma-Gamma random variables with generalized pointing errors. This study accounts for the attenuation effects that occur in moderate haze. The simulations use the system configuration parameters listed in Table II, consistent with most existing FSO systems [7], [48].

Fig. 6 illustrates the ergodic capacity of MIMO FSO systems based on analytical, asymptotic, and simulations evaluations as functions of the average SNR,  $\gamma_0$ , considering different numbers of transmitters, receivers, and different values for the non-zero boresight pointing error under conditions of moderate turbulence

TABLE II  
FSO SYSTEM CONFIGURATION PARAMETERS

Parameter	Values
Wavelength, $\lambda$	1550 nm
Wavenumber, $\kappa$	$2\pi/\lambda$
Optoelectronic conversion factor, $\eta$	0.9
Link distance, $z$	3 km
Attenuation coefficient, $\sigma$	4.2850 dB/km
Receiver aperture radius, $R_a$	5 cm
Transmit divergence angle, $\theta_z$	0.66 mrad
Beam width at 3 km, $w_z$	330 cm
Maximum jitter at 3 km, $\sigma_s$	55 cm

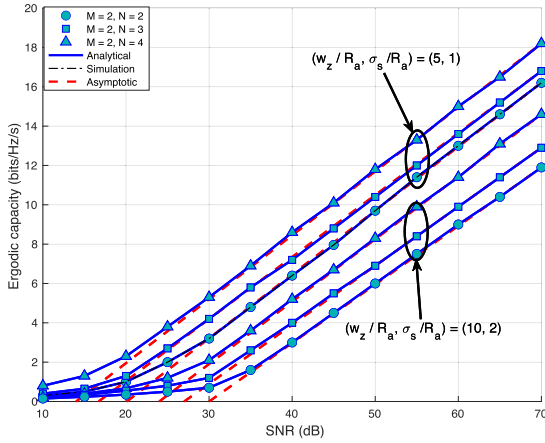


Fig. 6. The ergodic capacity of MIMO FSO systems for different combinations of  $M$ ,  $N$  numbers, and pointing error values.

with  $C_n^2 = 1.7 \times 10^{-14} \text{m}^{-2/3}$ . In this scenario, non-zero bore-sight pointing errors are considered with normalized beamwidth and jitter parameters of  $(w_z/R_a = 5, \sigma_s/R_a = 1)$ , and  $(w_z/R_a = 10, \sigma_s/R_a = 2)$ . The figure shows that the analytical expression in (25) and the asymptotic expression in (26) agree very well with the results of the Monte-Carlo simulation and thus confirm the accuracy of the proposed approximation. Remarkably, the derived analytical expression for the ergodic capacitance is very accurate over the entire range of SNR and agrees with the simulation results from low to high SNR values. As expected, increasing the number of receivers  $N$  leads to a remarkable enhancement in the ergodic capacity. For example, for  $(w_z/R_a, \sigma_s/R_a) = (10, 2)$  and  $\gamma_0$  of 70 dB, the ergodic capacity for a configuration of  $(M, N) = (2, 2)$  transmitters and receivers is 11.9 bits/Hz/s, which increases to 14.6 bits/Hz/s when the number of receivers is increased to  $N = 4$ . This is an example of how the MIMO approach can significantly mitigate the effects of pointing errors.

Fig. 7 shows the ergodic capacity of MIMO FSO systems in terms of average electrical SNR,  $\gamma_0$ , for different numbers of transmitters, receivers, and turbulence intensities when  $(w_z/R_a, \sigma_s/R_a) = (5, 1)$ , as well as results representing scenarios without pointing errors. The analysis of these curves shows a smaller variance  $\sigma_z^2$ , which leads to a higher ergodic capacity. For example, for  $(M, N) = (2, 2)$  and  $\gamma_0 = 70$  dB, the ergodic

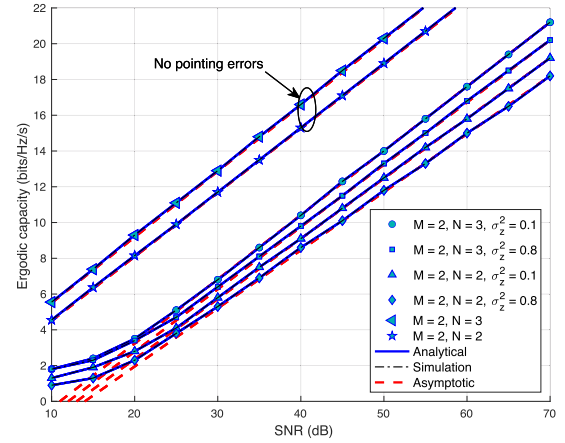


Fig. 7. The ergodic capacity of MIMO FSO systems for different turbulence intensities and  $M$ ,  $N$  numbers.

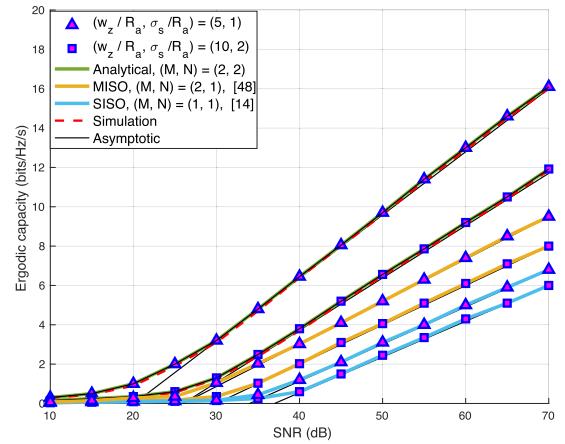


Fig. 8. The ergodic capacity versus SNR for different pointing error values with  $C_n^2 = 1.7 \times 10^{-14} \text{m}^{-2/3}$ .

capacity reaches 19.2 bits/Hz/s when  $\sigma_z^2$  is 0.1, compared to 18.1 bits/Hz/s for  $\sigma_z^2$  of 0.8. Additionally, the capacity increases significantly with a more significant number of receivers  $N$ . For example, for  $\sigma_z^2$  of 0.8 and  $\gamma_0$  of 70 dB, the ergodic capacity increases from 18.1 bits/Hz/s for  $N = 2$  to 20.2 bits/Hz/s for  $N = 3$ . Again, the result confirms that both the analytical expression in (25) and the asymptotic expression in (26) agree well with the Monte-Carlo simulations in all tested scenarios, including those without pointing errors, emphasizing the high accuracy of the approximation.

Furthermore, we have considered the models used in [14] and [48] to compare the results under moderate turbulence conditions, as shown in Fig. 8. The results obtained for the considered MIMO system are superior to those of the SISO model [14] and the MISO model [48]. For example, for  $(w_z/R_a, \sigma_s/R_a) = (5, 1)$  and  $\gamma_0$  of 70 dB, the ergodic capacity for the considered system with configuration  $(M, N) = (2, 2)$  is 15.9 bits/Hz/s, which decreases to 9.5 bits/Hz/s and 5.1 bits/Hz/s in the case of MISO and SISO systems, respectively.

Fig. 9 shows the outage probability of MIMO FSO systems for different configurations of transmitters and receivers considering the normalized jitter. The analytical expression in

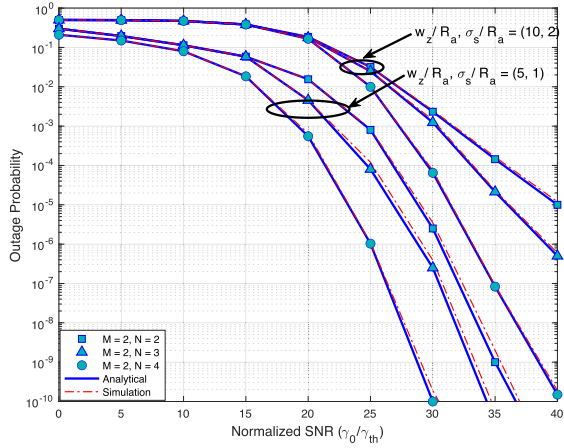


Fig. 9. The outage probability of MIMO FSO systems for different combinations of  $M$ ,  $N$ , and pointing error values.

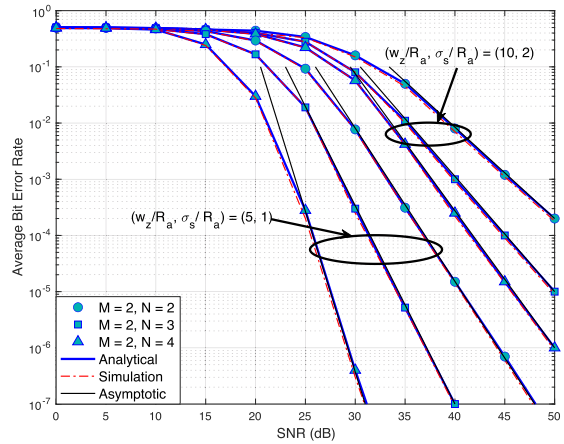


Fig. 10. The average BER performance of MIMO FSO systems for different combinations of  $M$ ,  $N$ , and pointing errors under moderate turbulence.

(30) correlates exceptionally well with the simulation results over the entire SNR range. As expected, the outage probability performance improves significantly as the number of receivers increases. For example, with a normalized beamwidth and jitter of  $(w_z/R_a, \sigma_s/R_a) = (10, 2)$  and an SNR of 30 dB, the outage probability for a configuration of  $(M, N) = (2, 2)$  is  $3 \times 10^{-6}$ , which drops significantly to  $1 \times 10^{-10}$  for  $(M, N) = (2, 4)$ .

Furthermore, the outage probability is  $3 \times 10^{-3}$  for  $(w_z/R_a, \sigma_s/R_a) = (5, 1)$  with  $(M, N) = (2, 2)$ , compared to  $6 \times 10^{-5}$  for  $(M, N) = (2, 4)$  at the same SNR. The results show that an increased normalized jitter has a negative effect on the outage probability. This finding is consistent with the results in [7] and [48].

Fig. 10 shows the average BER performance of MIMO FSO systems with different transmitters, receivers, and pointing error strength combinations. It is noticeable that the average BER improves significantly with smaller values for the beamwidth and jitter, especially with a higher number of  $M$  and  $N$ . For example, with  $(w_z/R_a, \sigma_s/R_a) = (5, 1)$  and  $\gamma_0$  of 30 dB for  $(M, N) = (2, 4)$  the average BER is  $5 \times 10^{-7}$ , as opposed to  $5 \times 10^{-2}$  for a system with  $(w_z/R_a, \sigma_s/R_a) = (10, 2)$ . The analytical results agree well with the low to medium SNR range

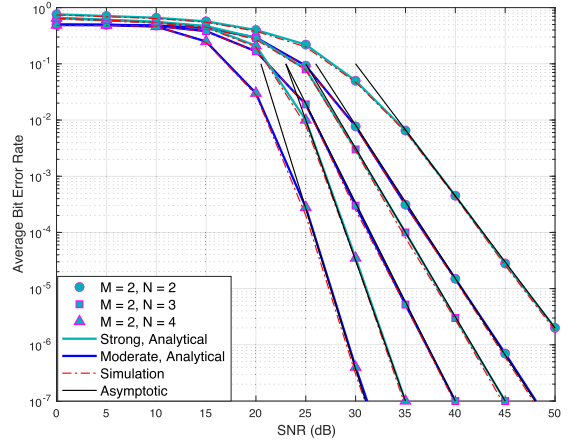


Fig. 11. The average BER performance of MIMO FSO systems for different combinations of  $M$ ,  $N$ , and atmospheric turbulence.

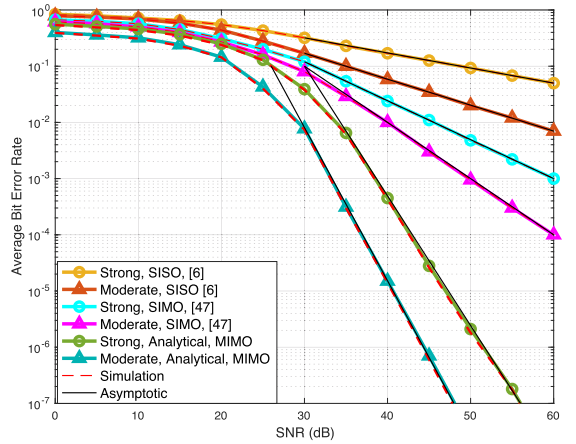


Fig. 12. The average BER versus SNR for different turbulence intensities.

simulation results and provide a lower limit for higher SNRs. The asymptotic BER performance shown in Fig. 10 confirms the validity of the expressions in (33) and (34).

Fig. 11 focuses on the average BER performance of a MIMO FSO system with  $(w_z/R_a, \sigma_s/R_a) = (10, 2)$  with different  $M$ ,  $N$  configurations, and turbulence intensities. The analytical expressions again show remarkable agreement with the simulation results over the entire SNR range for both moderate and strong turbulence, emphasizing the precision of (33). Furthermore, a significant decrease in average BER is observed when the number of receivers increases. Predictably, the average BER performance deteriorates under more severe turbulence. For example, to achieve an average BER of  $10^{-5}$  under strong turbulence with  $C_n^2 = 8 \times 10^{-14} \text{m}^{-2/3}$ , almost 6 dB more transmit power is required for an  $(M, N)$  configuration of (2, 2) than for moderate turbulence.

We have also considered the models used in [6] and [47] to compare the results under different turbulence conditions with  $(w_z/R_a, \sigma_s/R_a) = (10, 2)$ , as shown in Fig. 12. The results obtained for the considered scenario (MIMO) with  $(M, N) = (2, 2)$  are better than those of the SISO model used in [6] and the SIMO model in [47] with  $(M, N) = (1, 2)$  under all channel conditions. For example, to achieve an average BER of  $10^{-4}$



with moderate turbulence, almost 24 dB more transmit power is required for the SIMO system [47] than for the considered MIMO system. The analytical results consistently match the simulated results in all scenarios examined. This confirms the effectiveness of the proposed method in approximating the PDF of the sum of Gamma-Gamma variates with non-zero boresight pointing errors and atmospheric losses under different channel conditions. This novel method is also promising for evaluating performance in other widely recognized channel models, such as negative exponential, -K, and I-K, commonly used in congested urban wireless communication and satellite systems [59].

## VI. CONCLUSION

In this paper, the performance of MIMO FSO systems using the EGC scheme was investigated in the presence of the sum of Gamma-Gamma turbulence with non-zero boresight pointing errors and atmospheric attenuation. We have developed a novel analytical PDF approximation for this channel model. The accuracy of this approximation is substantiated by the KS test over a wide range of channel conditions. Using the derived statistical formulas, we have formulated closed-form expressions for the ergodic capacity, the outage probability, and the average BER performance. The analytical expression for the ergodic capacity accurately reflects the Monte-Carlo simulations for all SNR values. The asymptotic ergodic capacity has illustrated the influence of the system parameters. In addition, the outage probability and average BER results in all SNR ranges prove to be very accurate and serve as reliable lower bounds at high SNR values.

## APPENDIX A

Equation (15) can be written as the following

$$R_Q(r) = \sum_{q=Q+1}^{\infty} \frac{\left(\frac{s}{2\sigma_s^2}\right)^q (Ls)^{L+2q-1}}{q! \Gamma(L+q)} \left(\frac{r}{2\sigma_s^2}\right)^{L+2q-1} \times \exp\left(\frac{-Ls^2 - r^2}{2\sigma_s^2}\right) \quad (37)$$

To simplify further, (37) can then be represented as follows

$$R_Q(r) < \sum_{q=Q+1}^{\infty} \frac{\left(\frac{s}{2\sigma_s^2}\right)^q \left(\frac{Ls}{2\sigma_s^2}\right)^{L+2q-1} (\sigma_s^2 (2L+q-1))^{L+2q-1}}{q! \Gamma(L+q)} \times \exp\left(-\frac{Ls^2 + (\sigma_s^2 (L+2q-1))}{2\sigma_s^2}\right) \quad (38)$$

Now, by applying the Stirling asymptotic formula [54, Eq. (8.327.2)], (38) can be rewritten as

$$R_Q(r) < \frac{\left(\frac{Ls^2}{2\sigma_s^2}\right)^{Q+1} \left(\frac{Ls^2}{2\sigma_s^2}\right)^{L+1}}{(Q+1)! \sqrt{2\pi} (L+Q)} \frac{Q+2}{Q+2 - \left(\frac{Ls^2}{2\sigma_s^2}\right)} \exp\left(-\frac{Ls^2}{2\sigma_s^2}\right) \quad (39)$$

For further simplification, [39] can then be written as follows

$$R_Q(r) < \frac{\left(\frac{Ls^2}{2\sigma_s^2}\right)^{Q+1} \left(\frac{Ls^2}{2\sigma_s^2}\right)^{L+1}}{\sqrt{2\pi} (Q+1) \sqrt{2\pi} (L+Q)} \left(\frac{Ls^2 \exp(1)}{2\sigma_s^2 (Q+1)}\right)^{Q+1} \quad (40)$$

The first equality in (40) holds according to (41), which means that  $u = n / \left(\frac{1}{2\sigma_s^2}\right)$  maximizes  $r^{L+2q-1} \exp\left(\frac{-r^2}{2\sigma_s^2}\right)$  independently of  $r$ , and  $n$ .

$$\frac{dr^{L+2q-1} \exp\left(\frac{-r^2}{2\sigma_s^2}\right)}{dr} = 0 \Rightarrow r = \sigma_s^2 (L+2q-1) \quad (41)$$

The Stirling asymptotic formula [[54], Eq. (8.327.2)] can be used to derive the third and fifth inequalities, provided that  $Q$  is large enough. In addition, the fourth inequality applies due to

$$\begin{aligned} \sum_{q=Q+1}^{\infty} \frac{\left(\frac{Ls^2}{2\sigma_s^2}\right)^q}{q!} &= \frac{\left(\frac{Ls^2}{2\sigma_s^2}\right)^{Q+1}}{(Q+1)!} \left(1 + \frac{\left(\frac{Ls^2}{2\sigma_s^2}\right)}{Q+2} + \frac{\left(\frac{Ls^2}{2\sigma_s^2}\right)^2}{(Q+2)(Q+2)} \right. \\ &\quad \left. + \frac{\left(\frac{Ls^2}{2\sigma_s^2}\right)^3}{(Q+2)(Q+3)(Q+4)} \dots\right) \\ &< \frac{\left(\frac{Ls^2}{2\sigma_s^2}\right)^{Q+1}}{(Q+1)!} \left(1 + \frac{\left(\frac{Ls^2}{2\sigma_s^2}\right)}{Q+2} + \frac{\left(\frac{Ls^2}{2\sigma_s^2}\right)^2}{(Q+2)^2} \right. \\ &\quad \left. + \frac{\left(\frac{Ls^2}{2\sigma_s^2}\right)^3}{(Q+2)^3} + \dots\right) \\ &< \frac{\left(\frac{Ls^2}{2\sigma_s^2}\right)^{Q+1}}{(Q+1)!} \frac{Q+2}{Q+2 - \left(\frac{Ls^2}{2\sigma_s^2}\right)} \text{if } Q+2 > \left(\frac{Ls^2}{2\sigma_s^2}\right) \end{aligned} \quad (42)$$

## APPENDIX B

The ergodic capacity of the MIMO FSO systems can be expressed as

$$C = \frac{1}{\ln 2} \int_0^{\infty} \ln\left(1 + \frac{\gamma_0 t^2}{N}\right) f_{\bar{T}}(t) dt \quad (43)$$

where the series representation of  $f_{\bar{T}}(t)$  is shown in (21). In order to evaluate the above integral, we can express the natural logarithm in terms of Meijer's G-function [[54], Eq. (8.4.6.5)] as

$$\ln(1+x) = G_{2,2}^{1,2}\left(x \mid \begin{matrix} 1, 1 \\ 1, 0 \end{matrix}\right) \quad (44)$$

By incorporating (21) and (44) into (43), we have

$$\begin{aligned} C &= \frac{\sum_{q=0}^Q 2(ab)^{\frac{a+b}{2}} \left(\frac{sL}{2\sigma_s^2}\right)^{L+2q+1} \Gamma\left(\frac{L+2q+1}{2}\right)}{q! 2^{2L+q-1} \pi \ln 2 \Gamma(a) \Gamma(b) \omega^{\frac{a+b}{2}} A_0 I^a \Gamma(L+q)} \\ &\quad \times \exp(\zeta^2) \zeta^{4L+2q-2} \left(\frac{ab}{2A_0 I^a \omega}\right)^{\frac{a+b+3}{2}} \int_0^{\infty} t^{\frac{L+2q+a+b+4}{2}-1} \\ &\quad \times G_{2,2}^{1,2}\left(\frac{\gamma_0 t^2}{N} \mid \begin{matrix} 1, 1 \\ 1, 0 \end{matrix}\right) G_{L+2q+1, 2L+q+1}^{L+2q+1, 0} \\ &\quad \left(\frac{abLt}{2A_0 I^a \omega} \mid \begin{matrix} \{1\}_{i=1}^L \\ \{\frac{a+b+3}{2}\}, \{0\}_{i=1}^L \end{matrix}\right) dt \end{aligned} \quad (45)$$

Then, applying the integral formula in [[60], Eq. (07.34.21.0013.01)], we can derive a closed-form expression for the ergodic capacity of MIMO FSO systems  $C$  as in (25).

Additionally, Meijer's G function can be expressed, at a very low value of its argument, in terms of basic elementary

functions via utilizing Meijer's G function expansion in [[61], Theorem 1.4.2, Eq. (1.4.13)] and  $\lim_{x \rightarrow 0^+} cFd [e; f; x] = 1$  (here  $cFd$  denotes the generalized hypergeometric function) [62] as

$$\lim_{z \rightarrow 0^+} G_{p,q}^{m,n} \left( z \mid \begin{matrix} a_1, \dots, a_n, \dots, a_p \\ b_1, \dots, b_n, \dots, b_p \end{matrix} \right) = \sum_{k=1}^n z^{a_k-1} \times \frac{\prod_{i=1, i \neq k}^n \Gamma(a_k - a_i) \prod_{i=1}^m \Gamma(1 + b_i - a_k)}{\prod_{i=n+1}^p \Gamma(1 + a_i - a_k) \prod_{i=m+1}^q \Gamma(a_k - b_i)} \quad (46)$$

where,  $a_k - a_i \neq 0, \pm 1, \pm 2, \dots$ ; ( $k, i = 1, \dots, n; k \neq i$ ) and  $a_k - b_i \neq 1, 2, 3, \dots$ ; ( $k = 1, \dots, n; i = 1, \dots, m$ ) [45].

## APPENDIX C

To find the outage probability of the MIMO FSO systems, we incorporate the PDF expression of (21) in (29) as

$$P_{out} = \frac{\sum_{q=0}^Q 2(ab)^{\frac{a+b}{2}} \left(\frac{sL}{2\sigma_s^2}\right)^{L+2q+1} \Gamma\left(\frac{L+2q+1}{2}\right) \exp(\zeta^2)}{q! 2^{L+2q-1} \pi \Gamma(a) \Gamma(b) \omega^{\frac{a+b}{2}} A_0 I^a \Gamma(L+q)} \times \zeta^{4L+2q-2} \left(\frac{ab}{2A_0 I^a \omega}\right)^{\frac{a+b+3}{2}} \int_0^{\sqrt{\frac{N\gamma_{th}}{\gamma_0}}} t^{\frac{L+2q+a+b+4}{2}-1} \times G_{L+2q+1, 2L+q+1}^{L+2q+1, 0} \left( \frac{abLt}{2A_0 I^a \omega} \mid \begin{matrix} \{1\}_{l=1}^L \\ \left\{\frac{a+b+3}{2}\right\}, \{0\}_{l=1}^L \end{matrix} \right) dt \quad (47)$$

Then, by applying the integral formula in [[56], (26)], using (2), and replacing  $\gamma$  with  $\gamma_{th}$ , we can derive a closed-form expression for the outage probability of MIMO FSO systems  $P_{out}$  as in (30).

## APPENDIX D

The average BER of the MIMO FSO systems can be found by representing the complementary error function,  $erfc(\cdot)$  in (32) [[54], Eq. (8.250.4)] using Meijer's G-function [[63], Eq. (8.4.14.2)] as

$$erfc(\sqrt{x}) = \frac{1}{\sqrt{\pi}} G_{1,2}^{2,0} \left( x \mid \begin{matrix} 1 \\ 1, 1/2 \end{matrix} \right) \quad (48)$$

By incorporating (48) into (32), we have the following

$$P_b = \frac{1}{2\sqrt{\pi}} \int_0^\infty G_{1,2}^{2,0} \left( \frac{\gamma_0 t^2}{4N} \mid \begin{matrix} 1 \\ 1, 1/2 \end{matrix} \right) f_T(t) dt \quad (49)$$

Then, by substituting (21) into (49), we have the following

$$P_b = \frac{\sum_{q=0}^Q (ab)^{\frac{a+b}{2}} \left(\frac{sL}{2\sigma_s^2}\right)^{L+2q+1} \Gamma\left(\frac{L+2q+1}{2}\right) \zeta^{4L+2q-2}}{q! 2^{L+2q-1} (\pi)^{\frac{3}{2}} \Gamma(a) \Gamma(b) \omega^{\frac{a+b}{2}} A_0 I^a \Gamma(L+q)} \times \exp(\zeta^2) \left(\frac{ab}{2A_0 I^a \omega}\right)^{\frac{a+b+3}{2}} \int_0^\infty t^{\frac{L+2q+a+b+4}{2}-1} \times G_{1,2}^{2,0} \left( \frac{\gamma_0 t^2}{4N} \mid \begin{matrix} 1 \\ 1, 1/2 \end{matrix} \right) G_{L+2q+1, 2L+q+1}^{L+2q+1, 0} \left( \frac{abLt}{2A_0 I^a \omega} \mid \begin{matrix} \{1\}_{l=1}^L \\ \left\{\frac{a+b+3}{2}\right\}, \{0\}_{l=1}^L \end{matrix} \right) dt \quad (50)$$

Now, by applying the integration formula in [[60], Eq. (07.34.21.0013.01)], we have a closed-form expression for the average BER as in (33). In (33), the parameters  $\alpha_4$ ,  $B_7$ , and  $B_8$

are defined as the following

$$\alpha_4 = \frac{\sum_{q=0}^Q 2(ab)^{\frac{a+b}{2}} \left(\frac{sL}{2\sigma_s^2}\right)^{L+2q+1} \Gamma\left(\frac{L+2q+1}{2}\right)}{q! 2^{L+2q+1} (\pi)^{\frac{3}{2}} \ln(2) \Gamma(a) \Gamma(b) \omega^{\frac{a+b}{2}} A_0 I^a \Gamma(L+q)} \quad (51)$$

$$B_7 = 1, \left\{ -\frac{L+2q-2a-2b+3}{4} \right\}, \left\{ -\frac{a+b+1}{4} \right\}_{l=1}^L \quad (52)$$

$$B_8 = 1, 0.5, \left\{ -\frac{L+2q+a+b-4}{4} \right\}_{l=1}^L \quad (53)$$

## REFERENCES

- [1] W. M. R. Shakir, J. Charafeddine, H. Hamdan, I. A. Alshabeeb, N. G. Ali, and I. E. Abed, "Security-reliability tradeoff analysis for multiuser FSO communications over a generalized channel," *IEEE Access*, vol. 11, pp. 53019–53033, 2023.
- [2] W. M. R. Shakir and R. A. A. Abdul Kareem, "On secure communications for FSO systems over generalized turbulence channels," in *Proc. IEEE Int. Symp. Meas. Netw.*, 2022, pp. 1–6.
- [3] A. Al-Habash, L. C. Andrews, and R. L. Phillips, "Mathematical model for the irradiance probability density function of a laser beam propagating through turbulent media," *Proc. SPIE*, vol. 40, no. 8, pp. 1554–1562, 2001.
- [4] S. Al-Ahmadi, "The Gamma-Gamma signal fading model: A survey," *IEEE Antennas Propag. Mag.*, vol. 56, no. 5, pp. 245–260, Oct. 2014.
- [5] P. S. Bithas, N. C. Sagias, P. T. Mathiopoulos, G. K. Karagiannidis, and A. A. Rontogiannis, "On the performance analysis of digital communications over generalized-K fading channels," *IEEE Commun. Lett.*, vol. 10, no. 5, pp. 353–355, May 2006.
- [6] F. Yang, J. Cheng, and T. A. Tsiftsis, "Free-space optical communication with non-zero boresight pointing errors," *IEEE Trans. Commun.*, vol. 62, no. 2, pp. 713–725, Feb. 2014.
- [7] R. Boluda-Ruiz, A. García-Zambrana, B. Castillo-Vázquez, and C. Castillo-Vázquez, "Impact of non-zero boresight pointing error on ergodic capacity of MIMO FSO communication systems," *Opt. Exp.*, vol. 24, no. 4, pp. 3513–3534, Feb. 2016.
- [8] I. I. Kim et al., "Wireless optical transmission of fast ethernet, FDDI, ATM, and ESCON protocol data using the teralink laser communication system," *Proc. SPIE*, vol. 37, pp. 3143–3155, Jun. 1998.
- [9] A. Farid and S. Hranilovic, "Outage capacity optimization for free-space optical links with pointing errors," *J. Lightw. Technol.*, vol. 25, no. 7, pp. 1702–1710, Jul. 2007.
- [10] H. Sandalidis, T. Tsiftsis, G. Karagiannidis, and M. Uysal, "BER performance of FSO links over strong atmospheric turbulence channels with pointing errors," *IEEE Commun. Lett.*, vol. 12, no. 1, pp. 44–46, Jan. 2008.
- [11] H. Sandalidis, T. Tsiftsis, and G. Karagiannidis, "Optical wireless communications with heterodyne detection over turbulence channels with pointing errors," *J. Lightw. Technol.*, vol. 27, no. 20, pp. 4440–4445, Oct. 2009.
- [12] W. Gappmair, S. Hranilovic, and E. Leitgeb, "Performance of PPM on terrestrial FSO links with turbulence and pointing errors," *IEEE Commun. Lett.*, vol. 14, no. 5, pp. 468–470, May 2010.
- [13] A. Garcia-Zambrana, B. Castillo-Vazquez, and C. Castillo-Vazquez, "Asymptotic error-rate analysis of FSO links using transmit laser selection over Gamma-Gamma atmospheric turbulence channels with pointing errors," *Opt. Exp.*, vol. 20, pp. 2096–2109, 2012.
- [14] I. S. Ansari, M.-S. Alouini, and J. Cheng, "Ergodic capacity analysis of free-space optical links with nonzero boresight pointing errors," *IEEE Trans. Wireless Commun.*, vol. 14, no. 8, pp. 4248–4264, Aug. 2015.
- [15] A. Upadhyaya, V. K. Dwivedi, and G. K. Karagiannidis, "On the effect of interference and misalignment error in mixed RF/FSO systems over generalized fading channels," *IEEE Trans. Commun.*, vol. 68, no. 6, pp. 3681–3695, Jun. 2020.
- [16] A. Upadhyaya, J. Gupta, V. K. Dwivedi, and M.-S. Alouini, "Impact of RF I/Q imbalance on interference-limited mixed RF/FSO TWR systems with non-zero boresight error," *IEEE Trans. Wireless Commun.*, vol. 10, no. 2, pp. 416–420, Feb. 2021.
- [17] R. A. A. Abdul Kareem and W. M. R. Shakir, "On secrecy capacity analysis of FSO communication systems under generalized Malaga-M turbulence," in *Proc. 2nd Int. Conf. Math., Appl. Sci., Inf. Commun. Technol.*, 2023, pp. 1–13.

- [18] M. Ijaz, Z. Ghassemlooy, J. Perez, V. Brazda, and O. Fiser, "Enhancing the atmospheric visibility and fog attenuation using a controlled FSO channel," *IEEE Photon. Technol. Lett.*, vol. 25, no. 13, pp. 1262–1265, Jul. 2013.
- [19] E. Zedini, Y. Ata, and M.-S. Alouini, "Improving performance of integrated ground-HAPS FSO communication links with MIMO application," *IEEE Photon. J.*, vol. 16, no. 2, Apr. 2024, Art. no. 7301214.
- [20] Z. Wang, W.-D. Zhong, S. Fu, and C. Lin, "Performance comparison of different modulation formats over free-space optical (FSO) turbulence links with space diversity reception technique," *IEEE Photon. J.*, vol. 1, no. 6, pp. 277–285, Dec. 2009.
- [21] E. Bayaki, R. Schober, and R. K. Mallik, "Performance analysis of MIMO free-space optical systems in Gamma-Gamma fading," *IEEE Trans. Commun.*, vol. 57, no. 11, pp. 3415–3424, Nov. 2009.
- [22] X. Song and J. Cheng, "Subcarrier intensity modulated MIMO optical communications in atmospheric turbulence," *J. Opt. Commun. Netw.*, vol. 5, no. 9, pp. 1001–1009, Sep. 2013.
- [23] R. A. Kamboj, R. K. Mallik, M. Agrawal, and R. Schober, "Diversity combining in FSO systems in presence of non-Gaussian noise," in *Proc. Int. Conf. Signal Process. Commun.*, 2012, pp. 1–5.
- [24] D. Chen, G. Huang, G. Liu, and Y. Lei, "Performance of adaptive subcarrier modulated MIMO wireless optical communications in Malaga turbulence," *Opt. Commun.*, vol. 435, pp. 265–270, 2019.
- [25] P. Kaur, V. K. Jain, and S. Kar, "Performance analysis of FSO array receivers in presence of atmospheric turbulence," *IEEE Photon. Technol. Lett.*, vol. 26, no. 12, pp. 1165–1168, Jun. 2014.
- [26] P. Kaur, V. K. Jain, and S. Kar, "Performance analysis of free space optical links using multi-input multi-output and aperture averaging in presence of turbulence and various weather conditions," *IET Commun.*, vol. 9, no. 8, pp. 1104–1109, 2015.
- [27] A. Garcia-Zambrana, C. Castillo-Vazquez, and B. Castillo-Vazquez, "Outage performance of MIMO FSO links over strong turbulence and misalignment fading channels," *Opt. Exp.*, vol. 19, no. 14, pp. 13480–13496, 2011.
- [28] G. K. Varotsos, H. E. Nistazakis, C. K. Volos, and G. S. Tombras, "FSO links with diversity pointing errors and temporal broadening of the pulses over weak to strong atmospheric turbulence channels," *Optik*, vol. 127, no. 6, pp. 3402–3409, 2016.
- [29] M. Al-Nahhal, T. Ismail, H. Selmy, and M. M. Elmesalawy, "BPSK based SIM-FSO communication system with SIMO over log-normal atmospheric turbulence with pointing errors," in *Proc. 19th Int. Conf. Transp. Opt. Netw.*, 2017, pp. 1–4.
- [30] T. Ismail, E. Leitgeb, Z. Ghassemlooy, and M. Al-Nahhal, "Performance improvement of FSO system using multi-pulse pulse position modulation and SIMO under atmospheric turbulence conditions and with pointing errors," *IET Netw.*, vol. 7, no. 4, pp. 165–172, 2018.
- [31] G. K. Varotsos, H. E. Nistazakis, W. Gappmair, G. G. Sandalidis, and G. S. Tombras, "SIMO subcarrier PSK FSO links with phase noise and non-zero boresight pointing errors over turbulence channels," *IET Commun.*, vol. 13, no. 7, pp. 831–836, 2019.
- [32] N. D. Chatzidiamantis, G. K. Karagiannidis, and D. S. Michalopoulos, "On the distribution of the sum of Gamma-Gamma variates and application in MIMO optical wireless systems," in *Proc. IEEE Glob. Telecommun. Conf.*, 2009, pp. 1–6.
- [33] N. D. Chatzidiamantis and G. K. Karagiannidis, "On the distribution of the sum of Gamma-Gamma variates and applications in RF and optical wireless communications," *IEEE Trans. Commun.*, vol. 59, no. 5, pp. 1298–1308, May 2011.
- [34] M. Miao and X. Li, "Novel approximate distribution of the sum of Gamma-Gamma variates with pointing errors and applications in MIMO FSO links," *J. Opt. Commun.*, vol. 486, May 2021, Art. no. 126780.
- [35] H. Lei, C. Gao, I. S. Ansari, Y. Guo, G. Pan, and K. A. Qaraqe, "On physical-layer security over SIMO generalized-K fading channels," *IEEE Trans. Veh. Technol.*, vol. 65, no. 9, pp. 7780–7785, Sep. 2016.
- [36] H. Lei, I. S. Ansari, Y. Gao, G. Pan, and K. A. Qaraqe, "Secrecy performance analysis of single-input multiple-output generalized-K fading channels," *Front. Inf. Technol. Electron. Eng.*, vol. 17, no. 10, pp. 1074–1084, 2016.
- [37] K. P. Peppas, "A simple, accurate approximation to the sum of Gamma-Gamma variates and applications in MIMO free-space optical systems," *IEEE Photon. Technol. Lett.*, vol. 23, no. 13, pp. 839–841, Jul. 2011.
- [38] E. Illi, F. E. Bouanani, and F. Ayoub, "On the distribution of the sum of Málaga-M random variables and applications," *IEEE Trans. Veh. Technol.*, vol. 69, no. 11, pp. 13996–14000, Nov. 2020.
- [39] M. Miao and X. Li, "Novel approximate distribution of the sum of lognormal-rician turbulence channels with pointing errors and applications in MIMO FSO links," *IEEE Photon. J.*, vol. 14, no. 4, Aug. 2022, Art. no. 7334715.
- [40] N. I. Miridakis and T. A. Tsiftsis, "EGC reception for FSO systems under mixture-Gamma fading channels and pointing errors," *IEEE Commun. Lett.*, vol. 21, no. 6, pp. 1441–1444, Jun. 2017.
- [41] A. Goel and R. Bhatia, "On the performance of mixed user diversity-RF/spatial diversity-FSO cooperative relaying AF systems," *Opt. Commun.*, vol. 477, 2020, Art. no. 126333.
- [42] A. Goel and R. Bhatia, "Hybrid RF/MIMO-FSO relaying systems over Gamma-Gamma fading channels," in *Proc. Int. Conf. Innov. Comput. Commun.*, 2020, pp. 607–615.
- [43] A. Goel, A. Upadhyay, and V. K. Dwivedi, "Diversity aided millimeter-wave/free space optical cooperative relaying systems," *Int. J. Commun. Syst.*, vol. 34, no. 4, 2021, Art. no. e4700.
- [44] W. M. R. Shakir and A. S. Mahdi, "Errors rate analysis of the hybrid FSO/RF systems over foggy-weather fading-induced channel," in *Proc. 4th Sci. Int. Conf. Najaf*, 2019, pp. 156–160.
- [45] I. S. Ansari, F. Yilmaz, and M.-S. Alouini, "Performance analysis of FSO links over unified Gamma-Gamma turbulence channels," in *Proc. 81st IEEE Veh. Technol. Conf.*, 2015, pp. 1–5.
- [46] K.-J. Jung, S. S. Nam, M.-S. Alouini, and Y.-C. Ko, "Unified finite series approximation of FSO performance over strong turbulence combined with various pointing error conditions," *IEEE Trans. Commun.*, vol. 68, no. 10, pp. 6413–6425, Oct. 2020.
- [47] G. K. Varotsos, H. E. Nistazakis, M. I. Petkovic, G. T. Djordjevic, and G. S. Tombras, "SIMO optical wireless links with nonzero boresight pointing errors over M-modeled turbulence channels," *Opt. Commun.*, vol. 403, pp. 391–400, 2017.
- [48] R. Boluda-Ruiz, A. García-Zambrana, B. Castillo-Vázquez, and C. Castillo-Vázquez, "On the capacity of MISO FSO systems over Gamma-Gamma and misalignment fading channels," *Opt. Exp.*, vol. 23, no. 17, pp. 22371–22385, Aug. 2015.
- [49] W. M. R. Shakir, J. Charafeddine, H. A. Satai, H. Hamdan, S. Haddad, and J. Sayah, "Opportunistic schedule selection for multiuser MIMO FSO communications: A security-reliability trade-off perspective," *IEEE Photon. J.*, vol. 15, no. 3, Jun. 2023, Art. no. 7900215.
- [50] D. K. Borah and D. G. Voelz, "Pointing error effects on free-space optical communication links in the presence of atmospheric turbulence," *J. Lightw. Technol.*, vol. 27, no. 18, pp. 3965–3973, Sep. 2009.
- [51] A. A. Farid and S. Hranilovic, "Diversity gain and outage probability for MIMO free-space optical links with misalignment," *IEEE Trans. Commun.*, vol. 60, no. 2, pp. 479–487, Feb. 2012.
- [52] B. Kumbhani and R. S. Kshetrimayum, *MIMO Wireless Communications Over Generalized Fading Channels*, 1st ed. Boca Raton, FL, USA: CRC Press, 2017.
- [53] M. Yacoub, "The  $\kappa$ - $\mu$  distribution and the  $\eta$ - $\mu$  distribution," *IEEE Antennas Propag. Mag.*, vol. 49, no. 1, pp. 68–81, Feb. 2007.
- [54] I. S. Gradshteyn and I. M. Ryzhik, *Table of Integrals, Series, and Products*, 7th ed. Burlington, MA, USA: Academic, 2007.
- [55] B. D. Carter and M. D. Springer, "The distribution of products, quotients and powers of independent H-function variates," *SIAM J. Appl. Math.*, vol. 33, no. 4, pp. 542–558, 1977.
- [56] V. S. Adamchik and O. I. Marichev, "The algorithm for calculating integrals of hypergeometric type functions and its realization in REDUCE system," in *Proc. Int. Symp. Symbolic Algebr. Computation.*, 1990, pp. 212–224.
- [57] A. Papoulis and S. U. Pillai, *Probability, Random Variables, and Stochastic Processes*, 4th ed. New York, NY, USA: McGraw Hill, 2002.
- [58] Z. Wang and G. B. Giannakis, "A simple and general parameterization quantifying performance in fading channels," *IEEE Trans. Commun.*, vol. 51, no. 8, pp. 1389–1398, Aug. 2003.
- [59] H. Bai and M. Atiquzzaman, "Error modeling schemes for fading channels in wireless communications: A survey," *IEEE Commun. Surveys Tuts.*, vol. 5, no. 2, pp. 2–9, 2003.
- [60] Wolfram Research, Inc., "The Wolfram functions site." 2001. [Online]. Available: <https://functions.wolfram.com/HypergeometricFunctions/MeijerG/21/02/03/01/0002/>
- [61] A. M. Mathai and R. K. Saxena, "Generalized hypergeometric functions with applications in statistics and physical sciences," in *Lecture Notes in Mathematics*, vol. 348, New York, NY, USA: Springer, 1973.
- [62] M. D. Renzo, A. Guidotti, and G. E. Corazza, "Average rate of downlink heterogeneous cellular networks over generalized fading channels: A stochastic geometry approach," *IEEE Trans. Commun.*, vol. 61, no. 7, pp. 3050–3071, Jul. 2013.
- [63] A. P. Prudnikov, Y. A. Brychkov, and O. I. Marichev, *Integrals and Series: Special Functions*. New York, NY, USA: Gordon and Breach, 1983.